GA-A14121
UC-77

STATIC TEST OF THE GAS-COOLED FAST BREEDER REACTOR CORE SUPPORT GRID PLATE: COMPARISON OF EXPERIMENTAL, ANALYTICAL, AND FINITE-ELEMENT MODELS

by
A. S. CHUANG, K. H. CHANG, and C. E. WASHINGTON

Prepared under
Contract EY-76-C-03-0167
Project Agreement No. 23
for the San Francisco Operations Office
Department of Energy

GENERAL ATOMIC PROJECT 3228
DATE PUBLISHED: OCTOBER 1977

GENERAL ATOMIC COMPANY

ABSTRACT

The primary function of the gas-cooled fast breeder reactor (GCFR) grid plate is to hold core assemblies firmly in position so that the reactivity insertion associated with the plate deflection is limited to a value which satisfies plant safety requirements. Consequently, grid plate deflection under pressure is of particular importance rather than stress, as in the case of most perforated plates. Analyses were carried out using the concept of an equivalent solid material, and the equivalent solid plate was treated as a transversely isotropic elastic body. The general solutions for the axial and radial displacements were derived for a simply supported plate subject to a uniform load. The solid rim effect was also included.

Experimental and finite-element models were used to confirm the theoretical results, and it was found that the three solutions are in good agreement, and the maximum axial displacement discrepancy between them is about 6%. The close agreement of the three models not only proves that the analytical derivation and finite-element model are correct, but also indicates that the equivalent Young's modulus E^* and equivalent Poisson's ratio V^* are accurate.

NOMENCLATURE

E	Young's modulus for isotropic material or Young's modulus in the plane of isotropy for transversely isotropic material
E_r, E_θ, E_z	Young's moduli with respect to the directions r, θ, and z
E'	Young's modulus in the plane perpendicular to the plane of isotropy for transversely isotropic material
E^*	Effective Young's modulus for equivalent solid plate
G	shear modulus for isotropic material or shear modulus in the plane of isotropy for transversely isotropic material
G_{rz}, $G_{r\theta}$, $G_{\theta z}$	shear moduli for planes parallel to the coordinates r0z, r0θ, and θ0z; 0 is the origin of the coordinate
G'	shear modulus in the plane perpendicular to the plane of isotropy for transversely isotropic material
G^*	effective shear modulus for equivalent solid plate
H	radial width of the solid ring or flange
h	thickness of grid plate
M	radial moment of plate
p	pressure load
Q	radial force of plate
R_0	radius of grid plate plus solid ring
R_1	radius of perforated plate or equivalent solid plate
r, θ, z	cylindrical coordinates
t	thickness of solid ring or flange

u_r, u_θ, w	displacements in r, θ, and z directions
V'	transverse shear of plate
$\gamma_{r\theta}$, γ_{rz}, $\gamma_{\theta z}$	shear strains in cylindrical coordinates
ε_r, ε_θ, ε_z	normal strains in cylindrical coordinates
η	ligament efficiency of perforated plate
σ_r, σ_θ, σ_z	normal stresses in cylindrical coordinates
$\tau_{r\theta}$, τ_{rz}, $\tau_{\theta z}$	shear stress in cylindrical coordinates
ν	Poisson's ratio for isotropic material or Poisson's ratio in the plane of isotropy for transversely isotropic material
ν_{rz}, $\nu_{r\theta}$, $\nu_{\theta z}$	Poisson's ratios which characterize the transverse compression for tension in the direction of the axis of the coordinate (thus, ν_{rz} is a coefficient which characterizes the decrease in the z direction for tension in the radial direction)
ν'	Poisson's ratio in the plane perpendicular to the plane of isotropy for transversely isotro py for transversely isotropic material
ν^*	effective Poisson's ratio for equivalent solid plate

CONTENTS

FIGURES

TABLES

1. INTRODUCTION

The core support for the gas-cooled fast breeder reactor (GCFR) is a perforated plate into which the reactor fuel and blanket assemblies are inserted and locked. The plate is suspended from a support cylinder, and the core assemblies extend downward from the perforated plate. The helium gas flows down through the grid plate, and the core pressure drop appears across it.

The primary function of the grid plate is to hold the fuel and blanket assembly accurately in position so that the reactivity change associated with core distortion due to deformation of the structure is minimized to an acceptable value set by plant safety requirements. As a result, the grid plate is a deflection-limited rather than stress-limited structural component. The secondary function of the grid plate is to carry the deadweight of the control rod drive and locking mechanisms, the deadweight of the upper shield assembly, and the flow-induced pressure load.

This report discusses the analytical, experimental, and numerical investigation of the axial displacement of the grid plate under a uniform pressure. In the analytical study, the equivalent solid material concept was used, and the equivalent solid plate (Refs. 1 through 3) was treated using a transversely isotropic elasticity theory (Ref. 4). The general solutions for the axial and radial displacements were derived for a simply supported plate subjected to a uniform load. The solid rim effect was also included.

The finite-element method was used for the numerical model. An axisymmetric solid-element model was chosen in which the elements were symmetric with the vertical axis. The effective elastic constants were taken from the ASME Boiler and Pressure Vessel Code (Ref. 5) and Ref. 6.

The scaled test model was made of 7075-T651 aluminum alloy and had a diameter of 508 mm (20 in.) and a thickness of 91.44 mm (3.6 in.). The perforated pattern consisted of triangular penetrations having a pitch of 26.16 mm (1.03 in.) and a hole diameter of 24.2 mm (0.953 in.). The axial displacement of the grid plate model was measured at 68.95-kPa (10-psi) intervals during pressurization to a maximum pressure of 413.68 kPa (60 psi) across the grid plate. The pressure and displacement at various locations on the grid plate were constantly monitored and recorded.

To reflect the actual support condition of the grid plate test model, a partially clamped effect introduced by the preloaded bolts was formulated. Since the results of the analytical and numerical models were based on a simply supported condition, it was necessary to introduce a partial edge clamping effect to modify the results before comparing them with test measurements.

2. THEORY AND DISPLACEMENT ANALYSIS OF GRID PLATE

2.1. MATHEMATICAL FORMULATION

A thick perforated plate was treated as a transversely isotropic solid disk; the stress and strain relationships can be written as

$$\left.\begin{aligned}
\varepsilon_r &= \frac{1}{E}\sigma_r - \frac{\nu}{E}\sigma_\theta - \frac{\nu'}{E'}\sigma_z \quad , \\
\varepsilon_\theta &= -\frac{\nu}{E}\sigma_r + \frac{1}{E}\sigma_\theta - \frac{\nu'}{E'}\sigma_z \quad , \\
\varepsilon_z &= -\frac{\nu'}{E'}\sigma_r - \frac{\nu'}{E'}\sigma_\theta + \frac{1}{E'}\sigma_z \quad , \\
\gamma_{rz} &= \frac{1}{G'}\tau_{rz} \quad , \\
\gamma_{\theta z} &= \frac{1}{G'}\tau_{\theta z} = 0 \quad , \\
\gamma_{r\theta} &= \frac{1}{G}\tau_{r\theta} = 0 \quad .
\end{aligned}\right\} \qquad (1)$$

Using these equations, the stresses of a simply supported plate subject to a uniformly distributed load can be expressed as follows:

$$\left.\begin{aligned}
\sigma_r &= \frac{3p}{4h^3}(3+\nu)(R^2 - r^2)z + pm\left[\left(\frac{z}{h}\right)^3 - \frac{3}{20}\left(\frac{z}{h}\right)\right] \quad , \\
\sigma_\theta &= \frac{3p}{4h^3}\left[(3+\nu)R^2 - (1+3\nu)r^2\right]z + pm\left[\left(\frac{z}{h}\right)^3 - \frac{3}{20}\left(\frac{z}{h}\right)\right] \quad , \\
\sigma_z &= \frac{p}{2}\left[-1 + 3\left(\frac{z}{h}\right) - 4\left(\frac{z}{h}\right)^3\right] \quad , \\
\tau_{rz} &= -\frac{3p}{4h}r\left[1 - 4\left(\frac{z}{h}\right)^2\right] \quad ,
\end{aligned}\right\} \qquad (2)$$

where

$$m = \frac{E}{1 - \nu}\left[\frac{1}{G'} - \frac{\nu'(3 + \nu)}{E'}\right] \quad .$$

Substituting Eq. 2 into Eq. 1 and rearranging the formulations yields

$$\frac{1}{E}\sigma_r - \frac{\nu}{E}\sigma_\theta - \frac{\nu'}{E}\sigma_z = \frac{3p}{4Eh^3}\left[(3 + \nu)(1 - \nu)R^2 - 3(1 - \nu^2)r^2\right]z + \frac{pm}{E}(1 - \nu)\left[\left(\frac{z}{h}\right)^3 - \frac{3}{20}\left(\frac{z}{h}\right)\right] - \frac{\nu'}{E'}\frac{p}{2}\left[-1 + 3\left(\frac{z}{h}\right) - 4\left(\frac{z}{h}\right)^3\right] \quad , \tag{3}$$

$$-\frac{\nu}{E}\sigma_r + \frac{1}{E}\sigma_\theta - \frac{\nu'}{E'}\sigma_z = \frac{3p}{4Eh^3}\left[(3 + \nu)(1 - \nu)R^2 - (1 - \nu^2)r^2\right]z + \frac{pm(1 - \nu)}{E}\left[\left(\frac{z}{h}\right)^3 - \frac{3}{20}\left(\frac{z}{h}\right)\right] - \frac{\nu'}{E'}\frac{p}{2}\left[-1 + 3\left(\frac{z}{h}\right) - 4\left(\frac{z}{h}\right)^3\right] \quad , \tag{4}$$

$$-\frac{\nu'}{E'}\sigma_r - \frac{\nu'}{E'}\sigma_\theta + \frac{1}{E'}\sigma_z = -\frac{3p}{4E'h^3}\left[2\nu'(3 + \nu)R^2 - 4\nu'(1 + \nu)r^2\right]z - \frac{2pm\nu'}{E'}\left[\left(\frac{z}{h}\right)^3 - \frac{3}{20}\left(\frac{z}{R}\right)\right] + \frac{p}{2E'}\left[-1 + 3\left(\frac{z}{h}\right) - 4\left(\frac{z}{h}\right)^3\right] \quad . \tag{5}$$

Since

$$\left.\begin{aligned} \varepsilon_r &= \frac{\partial u_r}{\partial r} \quad , \\ \varepsilon_\theta &= \frac{u_r}{r} \quad , \\ \varepsilon_z &= \frac{\partial w}{\partial z} \quad , \\ \gamma_{rz} &= \frac{\partial u_r}{\partial z} + \frac{\partial w}{\partial r} \quad , \end{aligned}\right\} \tag{6}$$

the radial displacement can be obtained as follows:

$$\begin{aligned} \frac{\partial u_r}{\partial r} = \frac{3p}{4Eh^3} &\left[(3+\nu)(1-\nu)R^2 - 3(1-\nu^2)r^2\right]z \\ &+ \frac{pm(1-\nu)}{E}\left[\left(\frac{z}{h}\right)^3 - \frac{3}{20}\left(\frac{z}{h}\right)\right] \\ &- \frac{\nu'}{E'}\frac{p}{2}\left[-1 + 3\left(\frac{z}{h}\right) - 4\left(\frac{z}{h}\right)^3\right] \quad , \end{aligned} \tag{7}$$

$$\begin{aligned} u_r = \frac{3p}{4Eh^3} &\left[(3+\nu)(1-\nu)R^2 r - (1-\nu^2)r^3\right]z \\ &+ \frac{pm(1-\nu)}{E}\left[\left(\frac{z}{h}\right)^3 - \frac{3}{20}\left(\frac{z}{h}\right)\right] \\ &- \frac{\nu'}{E'}\frac{p}{2}\left[-1 + 3\left(\frac{z}{h}\right) - 4\left(\frac{z}{h}\right)^3\right] r + f(z) \quad , \end{aligned} \tag{8}$$

where $f(z)$ is an integration constant.

Since

$$\varepsilon_\theta = \frac{u_r}{r} = \frac{3p}{4Eh^3}\left[(3+\nu)(1-\nu)R^2 - (1-\nu^2)r^2\right]z + \frac{pm(1-\nu)}{E}\left[\left(\frac{z}{h}\right)^3 - \frac{3}{20}\left(\frac{z}{h}\right)\right] - \frac{\nu' p}{2E'}\left[-1 + 3\left(\frac{z}{h}\right) - 4\left(\frac{z}{h}\right)^3\right] \quad , \tag{9}$$

then Eqs. 8 and 9 can be compared, and it is concluded that $f(z) \equiv 0$. Thus,

$$U_r = \frac{pr}{E}\left\{\frac{E\nu'}{2E'} + \frac{3(1-\nu)}{4h^3}\left[(3+\nu)R^2 - (1+\nu)r^2\right]z - \frac{3z}{20h}\left[m(1-\nu) + 10\,\frac{E}{E'}\,\nu'\right] + \frac{z^3}{h^3}\left[m(1-\nu) - 2\,\frac{E}{E'}\,\nu'\right]\right\} \quad . \tag{10}$$

From the relation $\varepsilon_z = \partial w/\partial z$,

$$\frac{\partial w}{\partial z} = -\frac{3p}{4E'h^3}\left[2\nu'(3+\nu)R^2 - 4\nu'(1+\nu)r^2\right]z - \frac{2pm\nu'}{E'}\left[\left(\frac{z}{h}\right)^3 - \frac{3}{20}\left(\frac{z}{h}\right)\right] + \frac{p}{2E'}\left[-1 + 3\left(\frac{z}{h}\right) - 4\left(\frac{z}{h}\right)^3\right] \quad . \tag{11}$$

By integrating Eq. 11 with respect to z, the axial displacement becomes

$$w = -\frac{3p}{8E'h^3}\left[2\nu'(3+\nu)R^2 - 4\nu'(1+\nu)r^2\right]z^2 - \frac{2pm\nu'}{E'}\left[\frac{z^4}{4h^3} - \frac{3z^2}{40h}\right] + \frac{p}{2E'}\left[-z + \frac{3z^2}{2h} - \frac{z^4}{h^3}\right] + g(r) \quad , \tag{12}$$

where g(r) is a function of r. Axial displacement may be solved by applying the relation

$$\gamma_{rz} = \frac{\partial u_r}{\partial z} + \frac{\partial w}{\partial r} = \tau_{rz} \quad ,$$

so that

$$\frac{dg}{dr} = -\frac{3p}{4Eh^3}\left[(3+\nu)(1-\nu)R^2 - (1-\nu^2)r^2\right]r + \left[-\frac{3p}{5G'h} + \frac{3\nu'(7-\nu)p}{20E'h}\right]r \quad . \tag{13}$$

By integration, the function g(r) becomes

$$g(r) = -\frac{3p}{16Eh^3}\left[2(3+\nu)(1-\nu)R^2r^2 - (1-\nu^2)r^4\right] + \frac{3p}{10h}\left[\frac{\nu'(7-\nu)}{4E'} - \frac{1}{G'}\right]r^2 + C \quad , \tag{14}$$

where C is an integration constant.

Substituting Eq. 14 into Eq. 12, the axial displacement w yields

$$w = -\frac{3p}{4E'h^3}\left[\nu'(3+\nu)R^2 - 2\nu'(1+\nu)r^2\right]z^2 - \frac{2pm\nu'}{E'}\left[\frac{z^4}{4h^3} - \frac{3z^2}{40h}\right] + \frac{p}{2E'}\left[-z + \frac{3z^2}{2h} - \frac{z^4}{h^3}\right] - \frac{3p}{16Eh^3}\left[2(3+\nu)(1-\nu)R^2r^2 - (1-\nu^2)r^4\right] + \frac{3p}{10h}\left[\frac{\nu'(7-\nu)}{4E'} - \frac{1}{G'}\right]r^2 + C \quad . \tag{15}$$

The constant C can be evaluated using the boundary condition

$$w\Big|_{\substack{r=R\\z=0}} = 0 \quad .$$

Thus,

$$C = \frac{3p}{16Eh^3}\left[2(3+\nu)(1-\nu)R^4 - (1-\nu^2)R^4\right] - \frac{3p}{10h}\left[\frac{\nu'(7-\nu)}{4E'} - \frac{1}{G'}\right]R^2 \quad . \tag{16}$$

After substituting C into Eq. 15 and simplifying the equation, w becomes

$$w = \frac{p}{64D}(R^2 - r^2)\left[\frac{5+\nu}{1+\nu}R^2 - r^2\right] + \frac{3p}{10h}\left[\frac{1}{G'} - \frac{\nu'(7-\nu)}{4E'}\right](R^2 - r^2) + \frac{pz}{E'}\left\{-\frac{1}{2} - \frac{3\nu' z}{4E'h^3}\left[(3+\nu)R^2 - 2(1+\nu)r^2\right] + \frac{3z}{20h}[m\nu' + 5] - \frac{z^3}{2h^3}[m\nu' + 1]\right\} \quad , \tag{17}$$

where

$$D = \frac{Eh^3}{12(1-\nu^2)} \quad .$$

For an isotropic material,

$$E = E' \quad ,$$
$$\nu = \nu' \quad ,$$
$$G = G' = \frac{E}{2(1+\nu)} \quad ,$$

$$m = \frac{E}{1 - \nu}\left[\frac{1}{G'} - \frac{\nu'(3 + \nu)}{E'}\right]$$

$$= \frac{E}{1 - \nu}\left[\frac{2(1 + \nu)}{E} - \frac{\nu(3 + \nu)}{E}\right]$$

$$= \frac{1}{1 - \nu}\left[2 + 2\nu - 3\nu - \nu^2\right]$$

$$= \frac{1}{1 - \nu}(2 + \nu)(1 - \nu) = 2 + \nu \quad .$$

Substituting these relations into Eqs. 10 and 17, the radial and axial displacements can be reduced to

$$\left.\begin{aligned} u_r &= \frac{pr}{E}\left\{\frac{\nu}{2} + \frac{3(1 - \nu)}{4h^3}\left[(3 + \nu)R^2 - (1 + \nu)r^2\right]z \right.\right. \\ &\quad \left. - \frac{3z}{20h}(2 + 9\nu - \nu^2) + \frac{z^3}{h^3}(2 + \nu - \nu^2)\right\} \quad , \\ w &= \frac{p}{64D}(R^2 - r^2)\left[\frac{5 + \nu}{1 + \nu}R^2 - r^2\right] + \frac{3p(8 + \nu + \nu^2)}{40Eh}(R^2 - r^2) \\ &\quad + \frac{pz}{E}\left\{-\frac{1}{2} - \frac{3\nu z}{4Eh^3}\left[(3 + \nu)R^2 - 2(1 + \nu)r^2\right]\right. \\ &\quad \left.\left. + \frac{3z}{20h}(5 + 2\nu + \nu^2) - \frac{z^3}{2h^3}(1 + \nu)^2\right\} \quad . \end{aligned}\right\} \quad (18)$$

The expressions in Eq. 18 are identical to those given by Love's mathematical theory of elasticity (Ref. 7).

2.2. COMPUTATIONAL MODELS

2.2.1. Finite-Element Model

2.2.1.1. Discussion. Conventional engineering structures can be visualized as an assemblage of structural elements interconnected at a discrete number

of nodal points. If the force-displacement relationships for the individual elements are known, it is possible, by using various well known techniques of structural analysis (Refs. 8, 9), to derive the properties and study the behavior of the assembled structure.

In an elastic continuum, the true number of interconnection points is infinite, and herein lies the biggest difficulty in the numerical solution. The concept of finite elements, as originally introduced by Turner et al. (Ref. 10) attempts to overcome this difficulty by assuming the real continuum to be divided into elements interconnected only at a finite number of nodal points at which some fictitious forces, representative of the distributed stresses actually acting on the element boundaries, are supposed to be introduced. If such an idealization is permissible, the problem is reduced to that of a conventional structure and can be subjected to numerical treatment.

2.2.1.2. Application. The finite-element analysis for the grid plate was accomplished using the SAPIV computer program, and a two-dimensional axisymmetric solid element symmetrical to the vertical axis was employed (Fig. 1). To be consistent, the finite-element model was arranged to be as similar as possible to the test model, and a refinement of the boundary conditions of the finite element was necessary to reflect the actual arrangement of the test fixture.

The perforated plate was replaced by an equivalent solid plate and the effective elastic constants were generated according to Refs. 5 and 6. The equivalent solid circular plate had a 228.6-mm (9-in.) radius and a 91.44-mm (3.6-in.) thickness. There were 79 nodes in half of the symmetric model, and the edge, a 25.4-mm (1-in.) wide solid ring, was modeled into 18 nodes (Fig. 1).

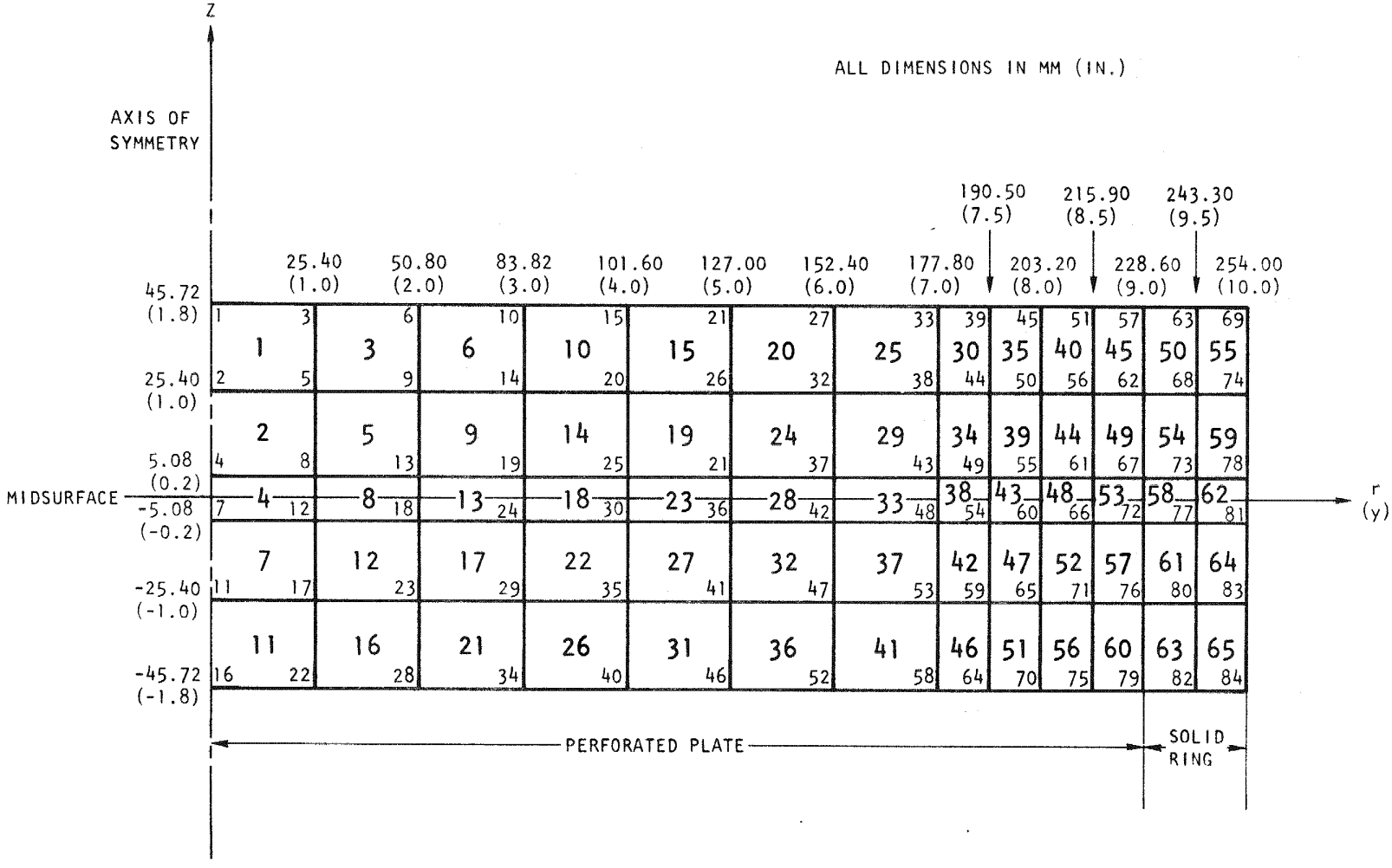

Fig. 1. Nodal arrangement of grid plate model, finite-element scheme

Based on Ref. 5, the in-plane effective elastic constants for an aluminum alloy can be determined as

$$E^* = 1.379 \times 10^3 \text{ MPa } (0.2 \times 10^6 \text{ psi}) \quad .$$

$$\nu^* = 0.76 \quad .$$

The effective elastic constants in the axial direction can be evaluated according to Ref. 6:

$$E' = 15.561 \times 10^3 \text{ MPa } (2.257 \times 10^6 \text{ psi}) \quad ,$$

$$G' = 3.105 \times 10^3 \text{ MPa } (0.4503 \times 10^6 \text{ psi}) \quad .$$

2.2.1.3. Orthotropic Material Properties. For a valid orthotropic material, the strain-stress matrix must satisfy the criteria of symmetry and positive definiteness. The strain-stress matrix for an orthotropic material can be written as

$$\begin{Bmatrix} \varepsilon_r \\ \varepsilon_z \\ \varepsilon_\theta \\ \gamma_{rz} \end{Bmatrix} = \begin{bmatrix} 1/Er & -\nu_{rz}/E_z & -\nu_{r\theta}/E_\theta & 0 \\ -\nu_{zr}/Er & 1/E_z & -\nu_{z\theta}/E_\theta & 0 \\ -\nu_{\theta r}/Er & -\nu_{\theta z}/E_z & 1/E_\theta & 0 \\ 0 & 0 & 0 & 1/G_{rz} \end{bmatrix} \begin{Bmatrix} \sigma_r \\ \sigma_z \\ \sigma_\theta \\ \tau_{rz} \end{Bmatrix} \quad . \quad (19)$$

To satisfy the symmetric condition, i.e.,

$$\left.\begin{aligned} \frac{\nu_{zr}}{E_r} &= \frac{\nu_{rz}}{E_z} \quad , \\ \frac{\nu_{r\theta}}{E_\theta} &= \frac{\nu_{\theta r}}{E_r} \quad , \\ \frac{\nu_{\theta z}}{E_z} &= \frac{\nu_{z\theta}}{E_\theta} \quad , \end{aligned}\right\} \quad (20)$$

the positive definiteness condition requires that all the cofactors in the determinant be positive:

$$\frac{1}{E_i} > 0 \quad , \qquad 1/G_{ij} > 0 \quad ,$$

$$1 - \nu_{ij}\nu_{ji} > 0 \quad , \qquad i,j = r,z,\theta \quad ,$$

or

$$\frac{1}{E_r}\frac{1}{E_z}\frac{1}{E_\theta} - \left(\frac{\nu_{zr}}{E_r}\right)\left(\frac{\nu_{\theta z}}{E_z}\right)\left(\frac{\nu_{r\theta}}{E_\theta}\right) - \left(\frac{\nu_{\theta r}}{E_\theta}\right)\left(\frac{\nu_{rz}}{E_z}\right)\left(\frac{\nu_{z\theta}}{E_\theta}\right)$$
$$- \left(\frac{1}{E_z}\right)\left(\frac{\nu_{\theta r}}{E_r}\right)\left(\frac{\nu_{r\theta}}{E_\theta}\right) - \left(\frac{\nu_{zr}}{E_r}\right)\left(\frac{\nu_{rz}}{E_z}\right)\left(\frac{1}{E_\theta}\right)$$
$$- \left(\frac{1}{E_r}\right)\left(\frac{\nu_{\theta z}}{E_z}\right)\left(\frac{\nu_{z\theta}}{E_\theta}\right) > 0 \quad . \qquad (21)$$

2.2.1.4. SAPIV Input Material Properties. The effective elastic constants of the equivalent solid plate can be obtained from Table 1 and the plots of Ref. 5. The SAPIV input material properties are as follows:

$$E_r = E_\theta = E^* = 1.379 \times 10^3 \text{ MPa } (0.2 \times 10^6 \text{ psi}) \quad ,$$

$$E_z = E' = 15.561 \times 10^3 \text{ MPa } (2.257 \times 10^6 \text{ psi}) \quad ,$$

$$G_{zr} = G^*_{zr} = 3.105 \times 10^3 \text{ MPa } (0.4503 \times 10^6 \text{ psi}) \quad ,$$

$$\nu_{zr} = \nu_{z\theta} = 0.3 \quad ,$$

$$\nu_{r\theta} = \nu^* = 0.76 \quad .$$

TABLE 1
VALUES OF G'/G AND E'/E FOR TRIANGULAR PENETRATION PATTERN[a]

η	G'/G	E'/E	η	G'/G	E'/E
0.0	0.0000	0.0931	0.4	0.5077	0.6735
0.05	0.0872	0.1815	0.5	0.6304	0.7733
0.1	0.1470	0.2654	0.6	0.7466	0.8549
0.15	0.2054	0.3448	0.7	0.8491	0.9184
0.2	0.2641	0.4196	0.8	0.9300	0.9637
0.25	0.3238	0.4899	0.9	0.9820	0.9909
0.3	0.3844	0.5556	1.0	1.000	1.000
0.333	0.4249	0.5965			

[a]These values are from Table 4.1 of Ref. 6.

The material used in the finite-element model can be shown to be a valid orthotropic material as follows:

$$\frac{1}{E_r} = \frac{1}{1.379 \times 10^3 \text{ MPa } (0.2 \times 10^6 \text{ psi})} = \frac{1}{E_\theta} > 0 \quad ,$$

$$1 - \nu_{r\theta}\nu_{\theta r} = 1 - (0.76)(0.76) > 0 \quad ,$$

$$\frac{1}{E_r E_\theta E_z}\left(1 - \nu_{r\theta}\nu_{\theta z}\nu_{zr} - \nu_{rz}\nu_{z\theta}\nu_{\theta r} - \nu_{zr}\nu_{rz} - \nu_{z\theta}\nu_{\theta z} - \nu_{r\theta}\nu_{\theta r}\right) > 0 \quad .$$

This implies that

$$1 - \nu_{r\theta}\nu_{\theta z}\nu_{zr} - \nu_{rz}\nu_{z\theta}\nu_{\theta r} - \nu_{zr}\nu_{rz} - \nu_{z\theta}\nu_{\theta z} - \nu_{r\theta}\nu_{\theta r} > 0 \quad ,$$

$$\nu_{\theta r} = \frac{\nu_{r\theta}}{E_r} E_\theta = \nu_{r\theta} = 0.76 \quad ,$$

$$\nu_{rz} = \frac{\nu_{zr}}{E_z} E_r = (0.3)\frac{1.379 \times 10^3 \text{ MPa } (0.2 \times 10^6 \text{ psi})}{15.561 \times 10^3 \text{ MPa } (2.257 \times 10^6 \text{ psi})} = 0.0265 \quad ,$$

$$\nu_{\theta z} = \frac{\nu_{z\theta}}{E_z} E_\theta = (0.3)\frac{1.379 \times 10^3 \text{ MPa } (0.2 \times 10^6 \text{ psi})}{15.561 \times 10^3 \text{ MPa } (2.257 \times 10^6 \text{ psi})} = 0.0265 \quad ,$$

$$\begin{aligned} &1 - (0.76)(0.0265)(0.3) - (0.0265)(0.3)(0.76) \\ &\quad - (0.3)(0.0265) - (0.3)(0.0265) - (0.76)(0.76) \\ &\quad = 1 - 0.0060 - 0.0060 - 0.079 - 0.079 - 0.5776 = 0.2524 > 0 \quad . \end{aligned}$$

2.2.1.5. Boundary Conditions. For the finite-element model, at 9.525 mm (3/8 in.) from the outer edge of the solid ring, the grid plate is simply supported around the circumference, and the boundary conditions of the grid plate are

At $r = 0$: $u_r = 0$, $\tau_{rz} = 0$;
At $r = 244.475$ mm (9.625 in.): $u_z = 0$, $\sigma_r = 0$;
At $z = 45.720$ mm (1.8 in.): $\sigma_z = -p$, $\tau_{rz} = 0$;
At $z = -45.720$ mm (-1.8 in.): $\sigma_z = 0$, $\tau_{rz} = 0$.

2.2.1.6. Results. The results of the finite-element analysis are shown in Fig. 2. The axial deflections of the grid plate subjected to pressures of 68.95 kPa (10 psi), 137.90 kPa (20 psi), 206.84 kPa (30 psi), 275.79 kPa (40 psi), 344.74 kPa (50 psi), and 413.68 kPa (60 psi) were plotted against the radial distance from the center of the plate. The 9.525-mm (3/8-in.) thick edge of the grid plate was clamped, and therefore there was no deflection at this point. The maximum axial deflection at the center of the grid plate subjected to a pressure of 413.68 kPa (60 psi) was 0.2337 mm (9.2×10^{-3} in.).

2.2.2. Analytical Model

2.2.2.1. Analytical Solution. The derivation of the axial displacement of the transversely isotropic plates subjected to a uniformly distributed pressure is shown in Section 2.1. According to Fig. 3, considering only the perforated plate, the axial displacement at the center of the plate can be written as

$$
\begin{aligned}
w = {} & \frac{p}{64D}\left(R_1^2 - r^2\right)\left[\frac{5 + \nu^*}{1 + \nu^*} R_1^2 - r^2\right] \\
& + \frac{3p}{10h}\left[\frac{1}{G'} - \frac{\nu'(7 - \nu^*)}{4E'}\right]\left(R_1^2 - r^2\right) \\
& + \frac{pz}{E'}\left\{-\frac{1}{2} - \frac{3\nu' z}{4E'h^3}\left[(3 + \nu^*)R_1^2 - 2(1 + \nu^*)r^2\right]\right. \\
& \left. + \frac{3z}{20h}(m\nu' + 5) - \frac{z^3}{2h^3}(m\nu' + 1)\right\} \quad . \qquad (22)
\end{aligned}
$$

However, the grid plate has an outer solid ring, and the effect of this ring can be divided into two parts: the subtractive displacement caused by the discontinuous moment M and the additional displacement caused by the discontinuous membrane force H and the edge rotation of the grid plate. A free-body diagram of the grid plate and the solid ring is shown in Fig. 4.

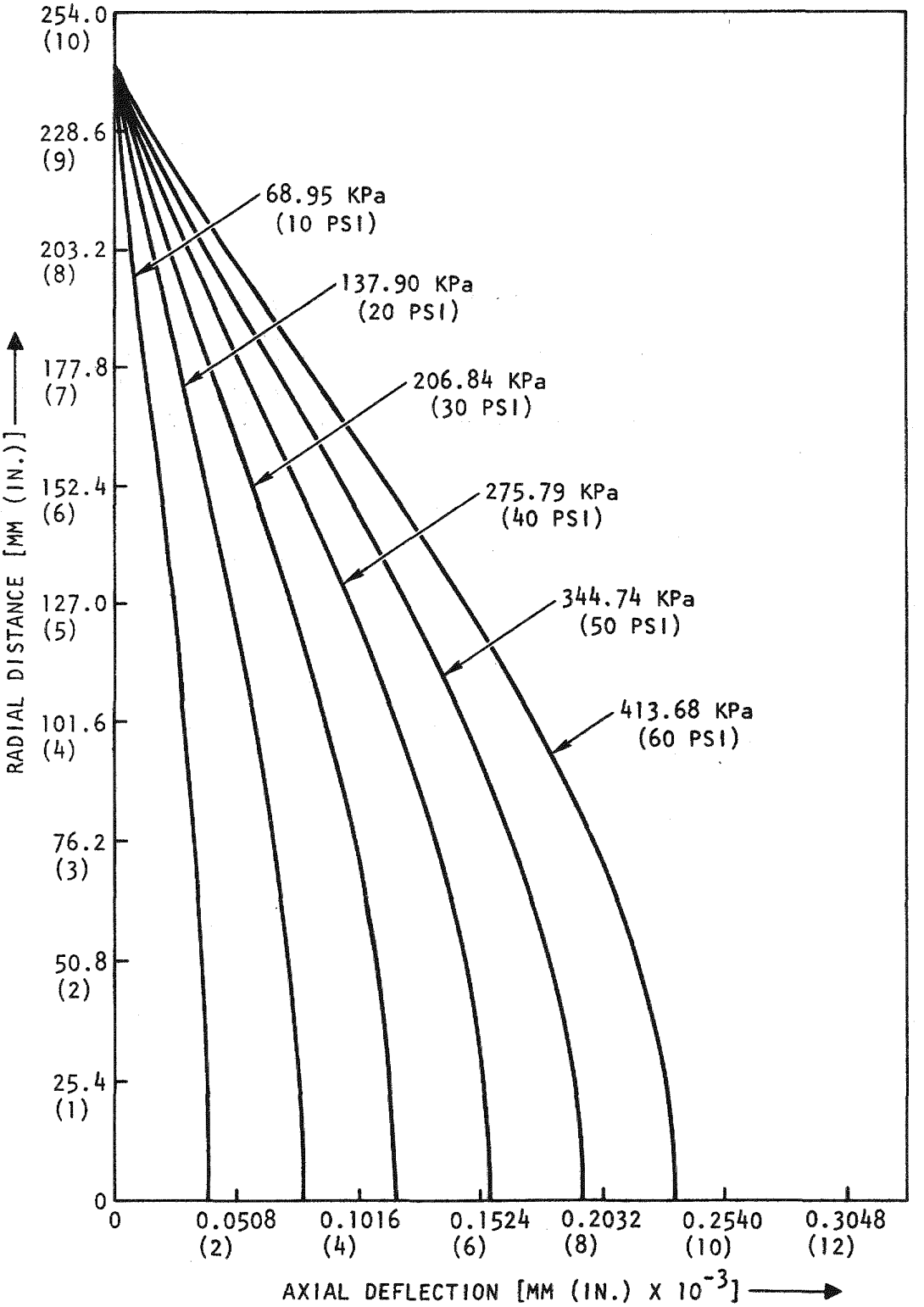

Fig. 2. Axial displacement of grid plate model by finite-element method

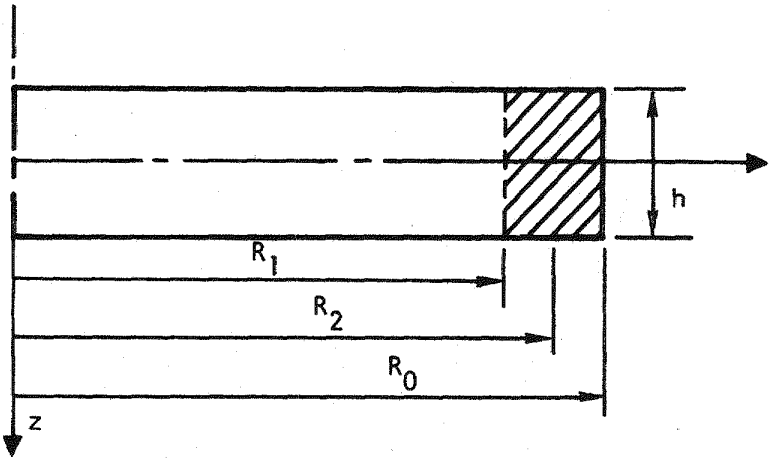

Fig. 3. Grid plate model and solid ring (R_2 is the radius from the center of the solid ring)

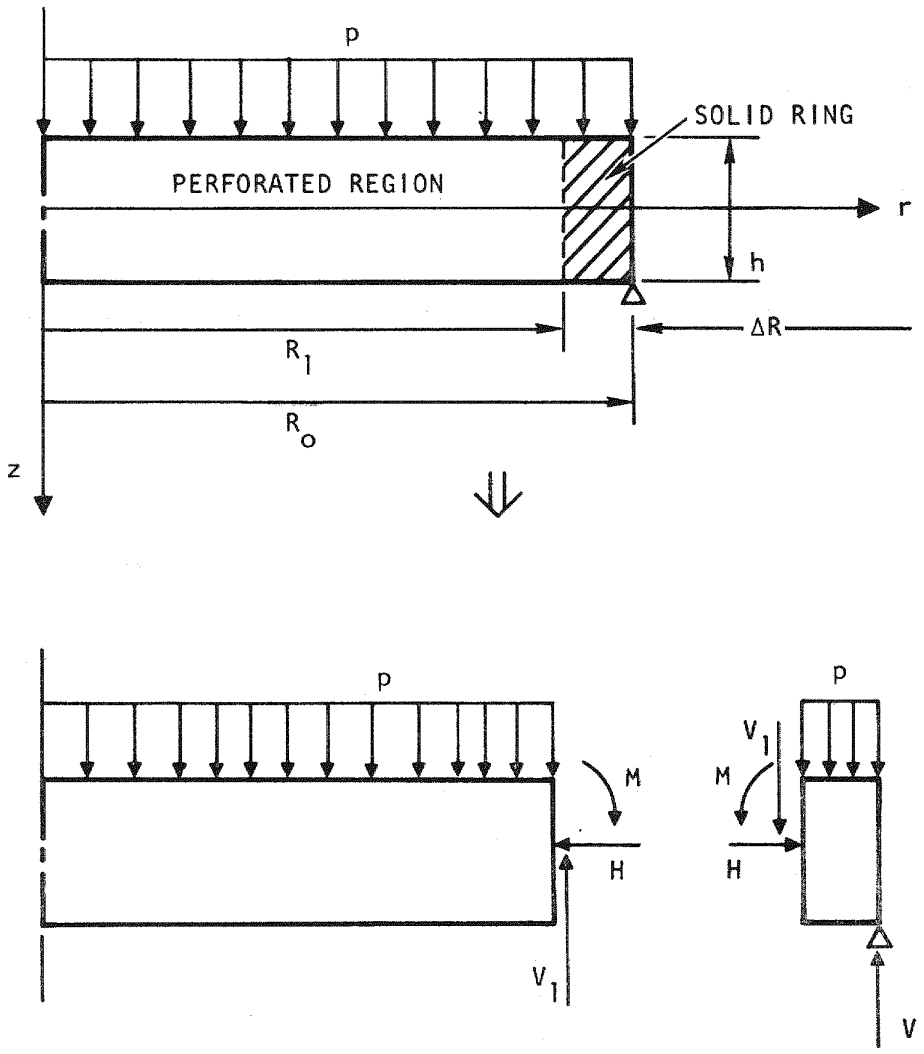

Fig. 4. Free-body diagram of the grid plate model and the solid ring

The displacement due to M can be written as

$$w_M = -\frac{6}{h^3}\left[\frac{(1-\nu')}{E'}(R^2 - r^2) - \frac{2\nu'}{E'} z^2\right] M \quad , \tag{23}$$

and the displacement due to H yields

$$w_H = \frac{2\nu'}{E'} \frac{z}{h} H \quad . \tag{24}$$

The extra displacement due to the edge rotation of the grid plate is

$$w_R = \frac{pR_2\Delta R^2(R_1^2 + R_0^2)}{4EI} \quad . \tag{25}$$

Therefore, the total displacement at the center of the grid plate is

$$\begin{aligned} w_{total} &= w + w_M + w_H + w_R \\ &= \frac{p}{64D}(R_1^2 - r^2)\left[\frac{5+\nu^*}{1+\nu^*} R_1^2 - r^2\right] \\ &\quad + \frac{3p}{10h}\left[\frac{1}{G'} - \frac{\nu'(7-\nu^*)}{4E'}\right](R_1^2 - r^2) \\ &\quad + \frac{pz}{E'}\left\{-\frac{1}{2} - \frac{3\nu' z}{4E'h^3}\left[(3+\nu^*)R_1^2 - 2(1+\nu^*)r^2\right]\right. \\ &\quad \left. + \frac{3z}{20h}(m\nu' + 5) - \frac{z^3}{2h^3}(m\nu' + 1)\right\} \\ &\quad - \frac{6}{h^3}\left[\frac{(1-\nu^*)}{E^*}(R_1^2 - r^2) - \frac{2\nu'}{E^*} z^2\right] M \\ &\quad + \frac{2\nu'}{E'} \frac{z}{h} H + \frac{pR_2(R_1^2 + R_0^2)\Delta R^2}{4EI} \quad , \end{aligned} \tag{26}$$

where

$$D = \frac{E^* h^3}{12(1 - \nu^{*2})} \quad ,$$

$$m = \frac{E^*}{1 - \nu^*}\left[\frac{1}{G'} - \frac{\nu'(3 + \nu^*)}{E'}\right] \quad .$$

The discontinuous moment M and membrane force H have been derived in Ref. 11 as

$$\left.\begin{aligned} M &= \frac{\dfrac{pR_1^3}{8D(1 + \nu^*)} - \dfrac{pR_2(R_1^2 + R_0^2)\Delta R}{4EI} + \dfrac{3pR_1}{5h}\left[\dfrac{1}{G'} - \dfrac{\nu'(7 - \nu^*)}{4E'}\right]}{\dfrac{R_1 R_2}{EI} + \dfrac{12R_1(1 - \nu^*)}{E^* h^3}} \quad , \\ H &= \frac{pEE^*\nu' h\Delta R}{2E'[E^* R_2 + (1 - \nu^*)E\Delta R]} \quad , \end{aligned}\right\} \qquad (27)$$

where

$$I = \frac{\Delta R h^3}{12} \quad .$$

Since the total displacement at the center of the grid plate under a uniform pressure loading p has been formulated in terms of the geometric and material parameters, it can be numerically calculated, providing the physical dimension, the configuration, and the material are known.

2.2.2.2. Numerical Results. The material elastic constants for aluminum alloy 7075-T651 are

$E = 68.947 \times 10^3$ MPa (10^7 psi),

$\nu = 0.3$,

$E^* = 1.379 \times 10^3$ MPa (0.2×10^6 psi),

$\nu^* = 0.76$,

$E' = 15.561 \times 10^3$ MPa (2.257×10^6 psi),

$G' = 3.105 \times 10^3$ MPa (0.4503×10^6 psi),

$\nu' = \nu = 0.3$.

The geometric dimensions of the grid plate are

$R_0 = 254.00$ mm (10 in.),

$R_1 = 228.60$ mm (9 in.),

$R_2 = 241.30$ mm (9.5 in.),

$h = 91.44$ mm (3.6 in.),

$\Delta R = R_0 - R_1 = 25.40$ mm (1.0 in.).

Based on the given elastic properties and geometric dimensions, the deflection at the center of the grid plate can be evaluated after a lengthy calculation and derivation. The final expression for the deflection can be written as

$$
\begin{aligned}
W(r,z,E^*,\nu^*) = {} & \frac{p(52257.96 - r^2)}{4077625.91E^*}\,[261289.8 - r^2 - 209031.84\nu^* \\
& - (52257.96 - r^2)\nu^{*2}] \\
& + (52257.96 - r^2)(0.945942 \times 10^{-12} + 0.015812 \times 10^{-12}\nu^*)p \\
& + \frac{pz}{E'}\left\{-0.5 - [(2.9649 \times 10^{-12} - 0.37824 \times 10^{-16}r^2)\right. \\
& + (0.9883 \times 10^{-12} - 0.37824 \times 10^{-16}r^2)\nu^*]z \\
& + \frac{0.8202 \times 10^{-2}(1 - \nu^*) + 0.130032 \times 10^{-12}E^* - 0.94877 \times 10^{-14}E^*\nu^*}{1 - \nu^*}\,z \\
& \left. - \frac{0.653975 \times 10^{-6}(1 - \nu^*) + 0.518388 \times 10^{-16}E^* - 0.0378239 \times 10^{-16}E^*\nu^*}{1 - \nu^*}\,z^3\right\}
\end{aligned}
$$

$$- \left[\frac{7.8477 \times 10^{-6}(52257.96 - r^2)(1 - \nu^*)}{E^*} - \frac{4.7086 \times 10^{-6} z^2}{E^*}\right] M$$

$$+ 0.421675 \times 10^{-12} zH + 4.073186 \times 10^{-8} p \quad ,$$

where

$$M = \frac{23.437 - 23.437\nu^* - 1.171132 \times 10^{-9} E^* + 7.229612 \times 10^{-12} E^* \nu^*}{3.58797 \times 10^{-3} - 3.58797 \times 10^{-3} \nu^* + 0.494356 \times 10^{-12} E^*} p \quad ,$$

$$H = \frac{8.81434 \times 10^{-10} E^*}{1 - \nu^* + 1.37787 \times 10^{-10} E^*} p \quad .$$

For a grid plate model with $E^* = 1.379 \times 10^3$ MPa (0.2×10^6 psi), $\nu^* = 0.76$ at $r = 0$ and $z = 0$, and a uniform pressure loading of 413.68 kPa (60 psi), the discontinuous moment M and discontinuous membrane force H yield:

$$M = 1.0772 \text{ MN·m/m (242.17 lb-in./in.)} \quad ,$$

$$H = 1.1693 \text{ kN/m (6.67 lb/in.)} \quad .$$

If M and H are substituted into the expression for the center displacement, then the numerical value of the displacement can be obtained:

$$W(0,0,1.379 \times 10^3 \text{ MPa}, 0.76)$$

$$= \frac{(413.68 \times 10^3)(52257.96)}{(4077625.909)(1.379 \times 10^9)} [261289.8 - (209031.84)(0.76)$$

$$- (52257.96)(0.76)^2]$$

$$+ 52257.96[0.945942 \times 10^{-12} + (0.158121 \times 10^{-13})(0.76)](413.68 \times 10^3)$$

$$- \frac{(7.8477 \times 10^{-6})(52257.96)(1 - 0.76)}{1.379 \times 10^9} (1.07721 \times 10^9)$$

$$+ (4.073186 \times 10^{-8})(413.68 \times 10^3)$$

$$= 2.77736 \times 10^{-1} + 2.07092 \times 10^{-2} - 7.68848 \times 10^{-2} + 1.685 \times 10^{-2}$$

$$= 0.2384 \text{ mm } (9.387 \times 10^{-3} \text{ in.}) \quad .$$

3. EXPERIMENTAL ANALYSIS OF GRID PLATE

3.1. TEST MODEL

The grid plate test model is shown in Fig. 5. The material used for the model is 7075-T651 aluminum alloy. The perforated pattern consists of triangular penetrations arranged in the form of a hexagonal assembly. There are 256 holes with a diameter of 24.206 mm (0.953 in.); the inner 118 holes are for the fuel assemblies, and the other 147 peripheral holes are for the blanket assemblies. The overall diameter of the grid plate model is 508.0 mm (20.0 in.), and it is 91.44 mm (3.6 in.) thick. The dimensions for the perforation and the boundary dividing the fuel and blanket assemblies are shown in Fig. 5.[†]

3.2. TEST FIXTURE

The test fixture is shown in Fig. 6, and its dimensions are listed below.

Upper ring

- Outside diameter = 508.0 mm (20 in.)
- Depth = 101.60 mm (4 in.)
- Wall thickness = 9.525 mm (3/8 in.)
- Material = steel

Lower ring

- Outside diameter = 508.0 mm (20 in.)
- Depth = 63.50 mm (2.5 in.)
- Wall thickness = 9.525 mm (3/8 in.)
- Material = steel

[†]The tests were conducted in the laboratory of the Department of Aerospace Engineering, San Diego State University, under the direction of Prof. R. Bedore.

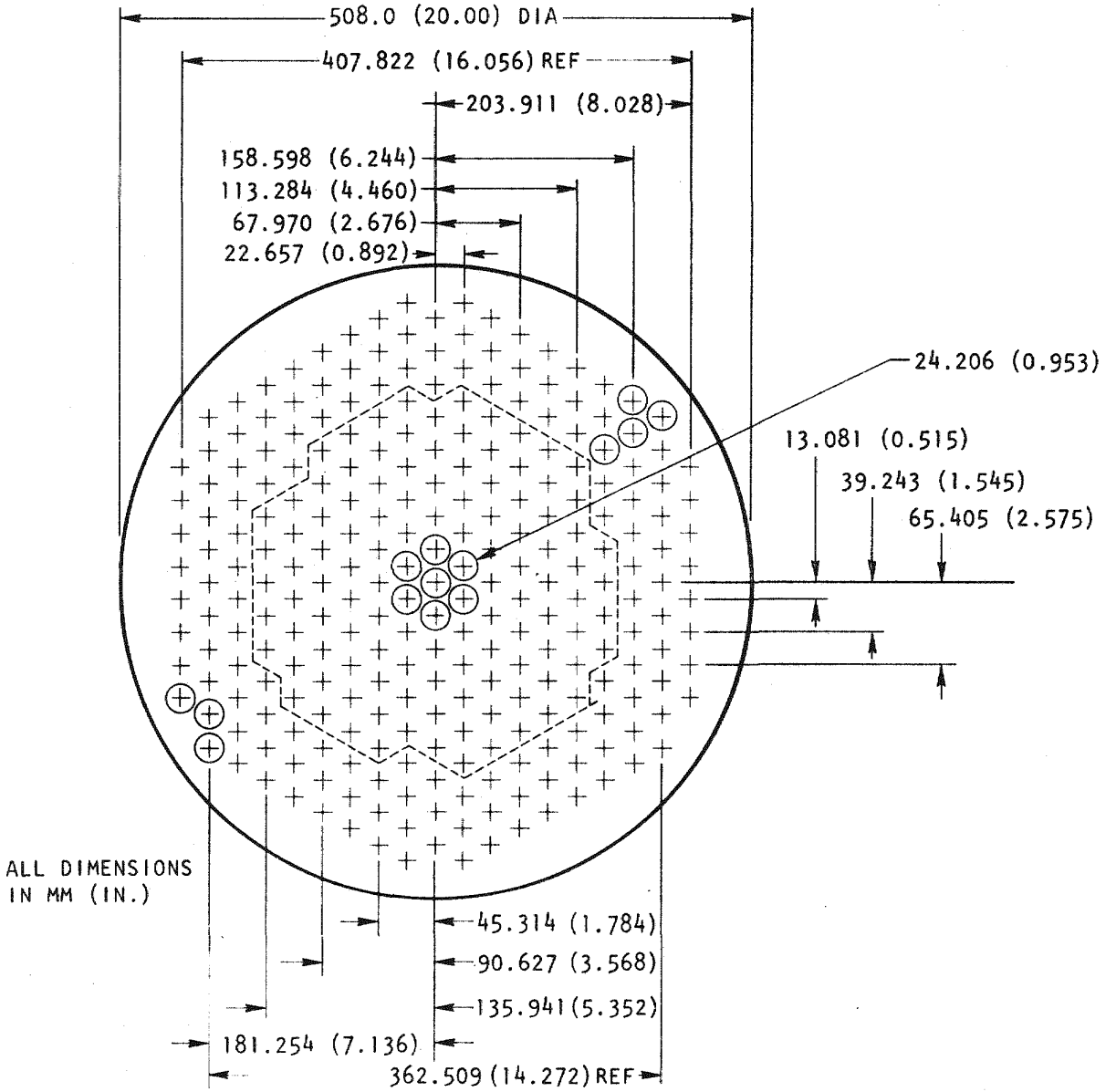

Fig. 5. Grid plate test model

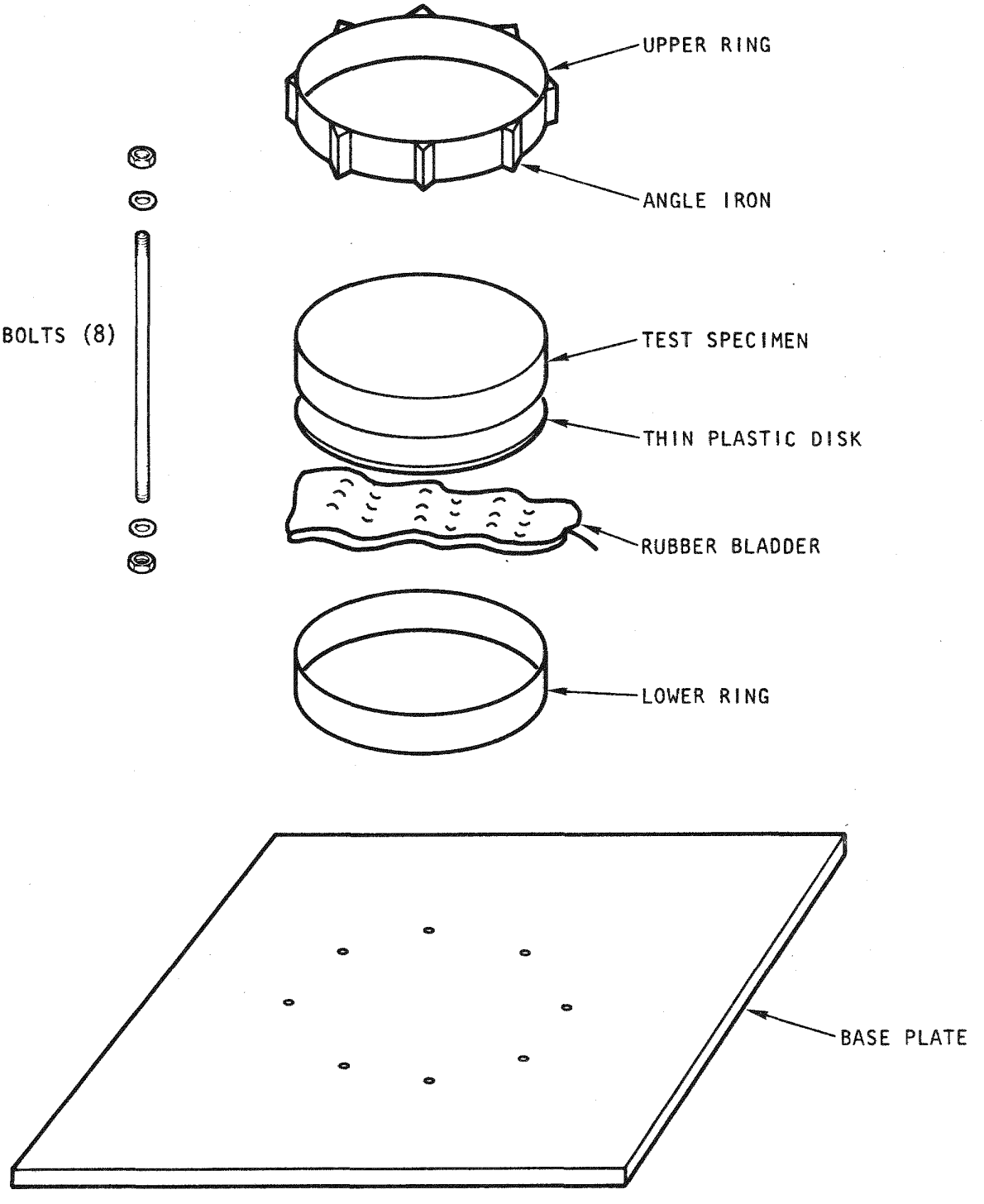

Fig. 6. Grid plate pressure-loading test fixture

Bladder

Truck tire tube size = 700-15

Plate

Size = 762.0 x 762.0 x 25.4 mm (30 x 30 x 1 in.)

Material = steel

Bolts (8)

Material = 12.70-mm (1/2-in.) diameter steel threaded at both ends with standard thread

Length of 5 bolts = 317.50 mm (12-1/2 in.)

Length of 3 bolts = 342.90 mm (13-1/2 in.)

As shown in Fig. 6, angles 609.60 mm (2 ft) x 50.80 mm (2 in.) x 6.35 mm (1/4 in.) steel are welded to the outside of the upper ring. There are eight angles equally spaced around the outer circumference. The upper ring is directly seated on the upper surface of the lower ring, and the rubber is placed inside the lower ring. A thin plastic disk [482.60 mm (19 in.) in diameter and approximately 4.763 mm (3/16 in.) thick] is placed on top of the bladder, directly under the specimen. This disk prevents the bladder from extruding into the tube holes. The lower ring sits directly on the base plate, and eight bolts connect the upper ring to the base plate, passing through the angles in the upper ring and the holes in the base plate. Nuts and washers are placed on both ends of the bolts and torqued to 67.791 N·m (50 ft-lb). Three of the bolts are 25.4 mm (1 in.) longer than the rest and are placed to form a tripod support for the whole assembly.

3.3. LOADING OF MODEL GRID PLATE

A uniform pressure load is applied to the lower half of the test specimen by pressurization of the bladder. The pressurization is accomplished by forcing water into the bladder with a hydraulic pump. A pressure guage is mounted in the pressure line from the pump to the bladder to enable a continual check on the hydraulic pressure in the system. The complete testing apparatus is placed on a rigid level base, which is the bottom part of a 1.3345×10^6 N (300,000-lb) testing machine.

3.4. CALIBRATION

The rigidity of the test fixture is indicated in Table 2, and the effect of the initial bolt torque on specimen (grid plate) deflection is given in Table 3. The point locations for a check on the rigidity of the test fixture are shown in Fig. 7 and the point locations for the effects of a bolt torque on specimen deflection are shown in Fig. 8.

The Marshalltown gauge located in the pressure line running from the hydraulic pump to the bladder was calibrated with a Crosby-Ashton deadweight tester. The calibration results are given in Table 4. Confirmation of the total pressure load being exerted on the grid plate model by the bladder was done by placing the lower ring, bladder, and grid plate assembly on a calibrated Riehle universal testing machine. The assembly was preloaded to 2224.1 N (500 lb) and then pressurized, and recordings of total load were made at 68.95-kPa (10-psi) pressure intervals up to 413.68 kPa (60 psi). The net load exerted on the grid plate by the bladder was then compared with theoretical values; the results are presented in Table 5.

3.5. TESTING

Testing was carried out in two parts. Part 1 was the static test of the grid plate model without tubes to obtain the axial deflection versus pressure plots (Figs. 9 through 11); the test setup and measuring point locations are shown in Figs. 12 and 13. Part 2 was the static test of the grid plate model using selected tubes which were inserted to obtain the radial deflection of the upper tube ends under pressure loadings; the test setup and measuring point locations are shown in Figs. 14 and 15. Measurements were taken with dial indicators attached to the head of the 1.3345×10^6 N (300,000-lb) testing machine (see Fig. 12). Each test consisted of setting the dial indicator gauges at zero and taking readings at 68.95-kPa (10-psi) intervals during pressurization to a maximum of 413.68 kPa (60 psi). The pressure was then reduced in 68.95-kPa (10-psi) intervals and recordings were taken as the pressure was relieved. Each test was

TABLE 2
CHECK ON RIGIDITY OF TEST FIXTURE[a]

Pressure [kPa (psi)]	Deflection [mm (10^{-3} in.)]							
	Point							
	1	2	3	4	5	6	7	8
0	0.0	0.0	0.0	0.0	0.0	0.0	0.0	0.0
68.95 (10)	0.0	0.0	0.0	0.0	0.0102 (0.4)	-0.0025 (-0.1)	0.0	0.0
137.90 (20)	0.0	0.0	0.0	0.0	0.0279 (1.1)	-0.0051 (-0.2)	0.0	0.0
206.84 (30)	0.0	0.0	0.0	0.0	0.0483 (1.9)	-0.0051 (-0.2)	0.0	0.0
275.79 (40)	0.0	0.0	0.0	0.0	0.0686 (2.7)	-0.0051 (-0.2)	0.0	0.0
344.74 (50)	0.0	0.0	0.0	0.0	0.0940 (3.7)	0.0	0.0	0.0
413.68 (60)	0.0	0.0	0.0	0.0	0.1168 (4.6)	0.0051 (0.2)	0.0025 (0.1)	0.0
344.74 (50)	0.0	0.0	0.0	0.0	0.1016 (4.0)	0.0025 (0.1)	0.0025 (0.1)	0.0
275.79 (40)	0.0	0.0	0.0	0.0	0.0838 (3.3)	0.0	0.0	0.0
206.84 (30)	0.0	0.0	0.0	0.0	0.0610 (2.4)	0.0	0.0	0.0
137.90 (20)	0.0	0.0	0.0	0.0	0.0406 (1.6)	0.0	0.0	0.0
68.95 (10)	0.0	0.0	0.0	0.0	0.0203 (0.8)	0.0	0.0	0.0
0	0.0	0.0	0.0	0.0	0.0	0.0	0.0	0.0

[a]Data taken on January 9, 1976; point locations shown in Fig. 7. Torque on test fixture bolt nuts = 67.791 N·m (50 ft-lb). Dial indicator gauge on points 5 and 7 have divisions of ten thousandths [0.00254 mm (0.0001 in.)]; all others, thousandths [0.0254 mm (0.001 in.)]. Readings are given in mils [0.0254 mm (0.001 in.)]. Referenced to head of 136,080-kg (300,000-lb) test machine.

TABLE 3
EFFECTS OF BOLT TORQUE ON SPECIMEN DEFLECTION[a]

Date	Bolt Torque [N·m (ft-lb)]	Deflection [mm (10^{-3} in.)]				
		Point				
		1	2	3	4	5
1/9/76	67.791 (50)	0.1194 (4.7)	0.0127 (0.5)	--[b]	0.0	0.0025 (0.1)
1/9/76	67.791 (50)	0.1194 (4.7)	0.0178 (0.7)	--	0.0	--
1/9/76	33.90 (25)	0.1499 (5.9)	--	--	0.0	0.0279 (1.1)
1/9/76	33.90 (25)	0.1346 (5.3)	--	--	0.0	--
1/15/76	13.558 (10)[c]	0.2235 (8.8)	0.0508 (2.0)	0.1270 (5.0)	--	--
1/16/76	13.558 (10)[c]	0.2261 (8.9)	0.0762 (3.0)	0.1016 (4.0)	--	--
1/16/76	13.558 (10)[c]	0.2159 (8.5)	0.0762 (3.0)	0.1270 (5.0)	--	--

[a]Point locations shown in Fig. 8. Dial indicator gauge on points 1 and 5 have divisions of ten-thousandths; all others, one-thousandths. Readings given in mils [0.0254 mm (0.001 in.)]. Referenced to head of 136,080-kg (300,000-lb) test machine. Pressure = 413.68 kPa (60 psi).

[b]No measurement taken.

[c]Measurable gap between lower ring and test specimen [greater than 0.381 mm (0.015 in.)].

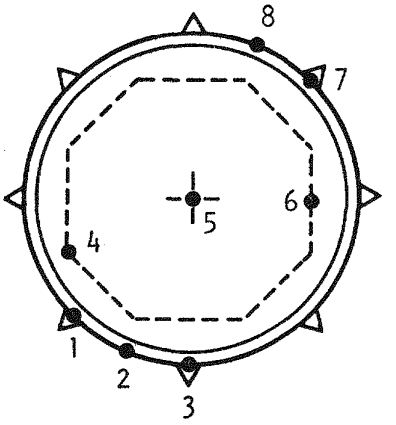

Fig. 7. Point locations for check on rigidity of test fixture

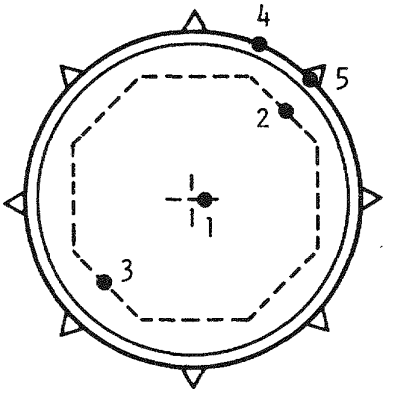

Fig. 8. Point locations for effects of bolt torque on specimen deflection

TABLE 4
PRESSURE GAUGE CALIBRATION[a]

Marshalltown Gauge[b] [kPa (psi)]	Crosby-Ashton Deadweight Tester [kPa (psi)]
24.13 (3.5)	34.47 (5)
68.95 (10)	68.95 (10)
106.87 (15.5)	103.42 (15)
137.90 (20)	137.90 (20)
172.37 (25)	172.37 (25)
206.84 (30)	206.84 (30)
241.32 (35)	241.32 (35)
275.79 (40)	275.79 (40)
310.26 (45)	310.26 (45)
341.29 (49.5)	344.74 (50)
375.76 (54.5)	379.21 (55)
413.69 (60)	413.69 (60)
444.71 (64.5)	448.16 (65)
479.19 (69.5)	482.63 (70)
510.21 (74)	517.11 (75)
544.69 (79)	551.58 (80)
579.16 (84)	586.05 (85)
613.63 (89)	620.53 (90)
648.11 (94)	655.00 (95)
679.13 (98.5)	689.48 (100)

[a] Data taken on November 25, 1975.

[b] 0 to 689.48 kPa (0 to 100 psi).

TABLE 5
TOTAL PRESSURE LOAD CALIBRATION[a]

Pressure [kPa (psi)]	Indicated Load [kg (lb)]	Indicated Load Minus Preload [kg (lb)]	Calculated Load [kg (lb)]
0	226.80 (500)	0	0
68.95 (10)	925.54 (2,100)	725.75 (1,600)	1319.95 (2,910)
137.90 (20)	2143.22 (4,725)	1916.43 (4,225)	2639.91 (5,820)
206.84 (30)	3481.32 (7,675)	3254.53 (7,175)	3959.86 (8,730)
275.79 (40)	4751.38 (10,475)	4524.58 (9,975)	5279.82 (11,640)
344.74 (50)	6078.14 (13,400)	5851.34 (12,900)	6599.77 (14,550)
413.68 (60)	7416.24 (16,350)	7189.44 (15,850)	7919.72 (17,460)
344.74 (50)	6146.18 (13,550)	5919.38 (13,050)	6599.77 (14,550)
275.79 (40)	4830.76 (10,650)	4603.96 (10,150)	5279.82 (11,640)
206.84 (30)	3583.38 (7,900)	3356.58 (7,400)	3959.86 (8,730)
137.90 (20)	2177.24 (4,800)	1950.45 (4,300)	2639.91 (5,820)
68.95 (10)	952.54 (2,100)	861.83 (1,900)	1319.95 (2,910)
0	226.80 (500)	0	0

[a]Data taken on December 4, 1975 using a Riehle universal testing machine. Preload = 226.80 kg (500 lb); calculated load = $(\pi/4)(488.95\ \text{mm})^2$ x pressure.

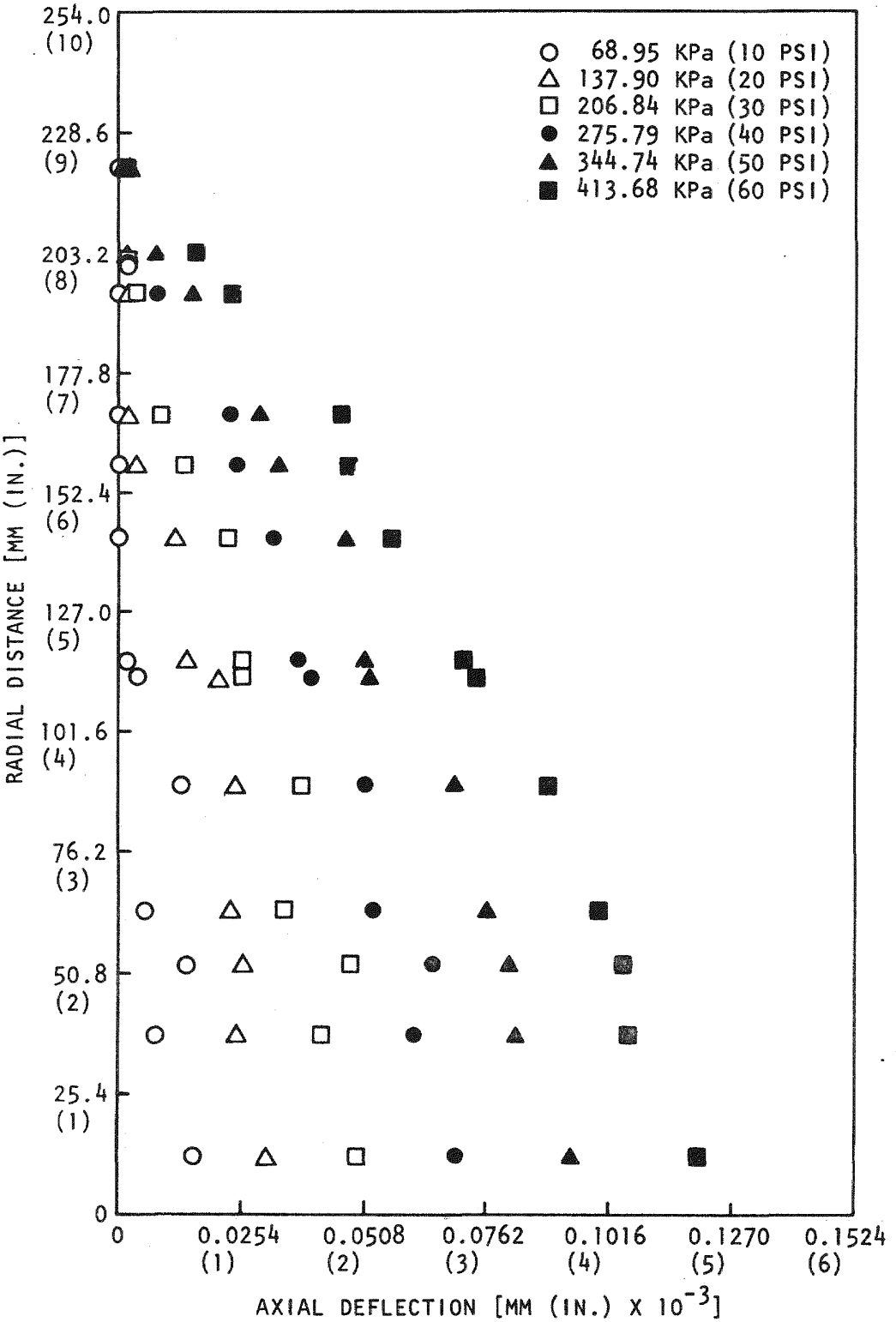

Fig. 9. Axial displacement vs radial distance of grid plate, loading case

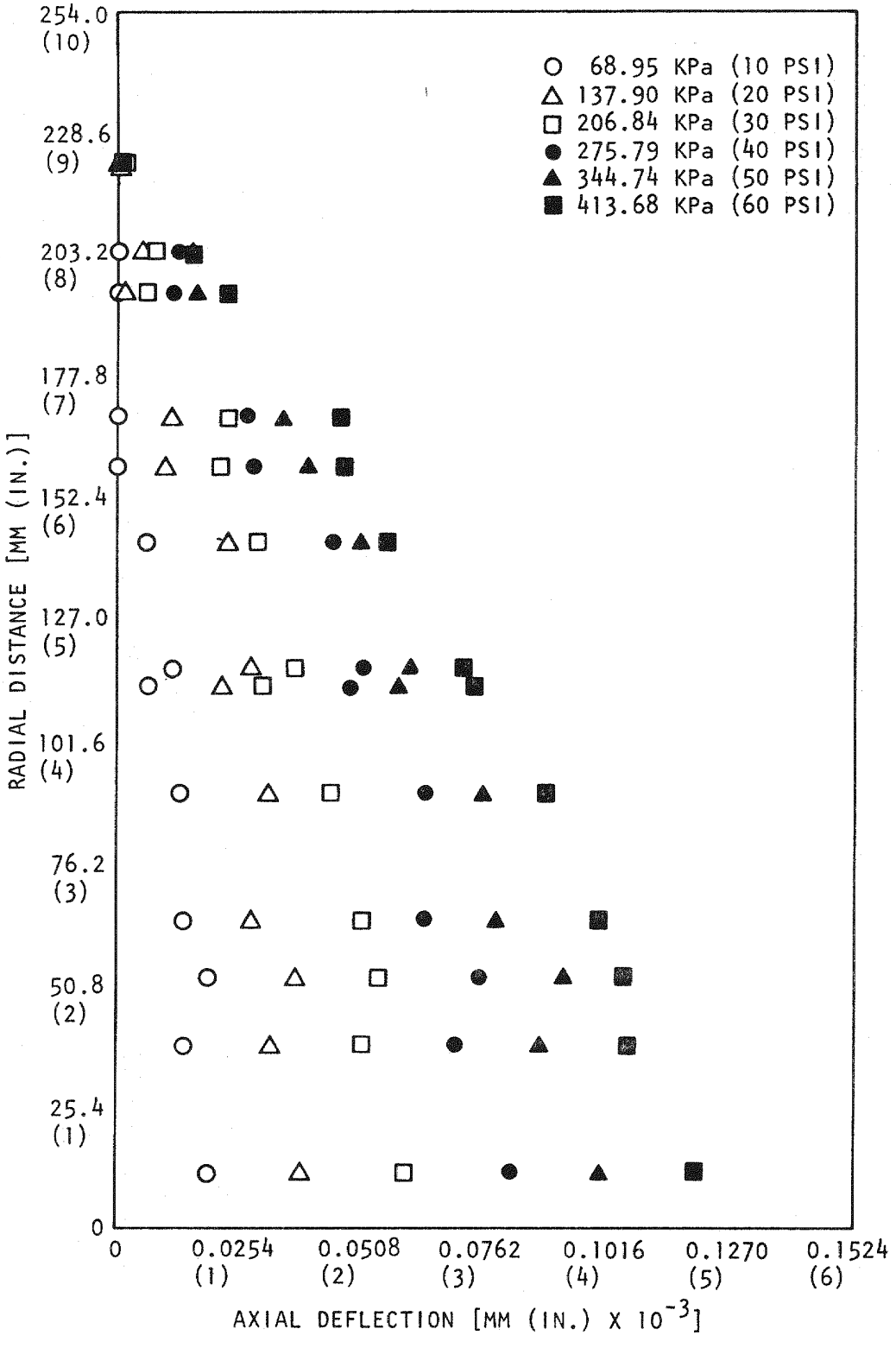

Fig. 10. Axial displacement vs radial distance of grid plate, unloading case

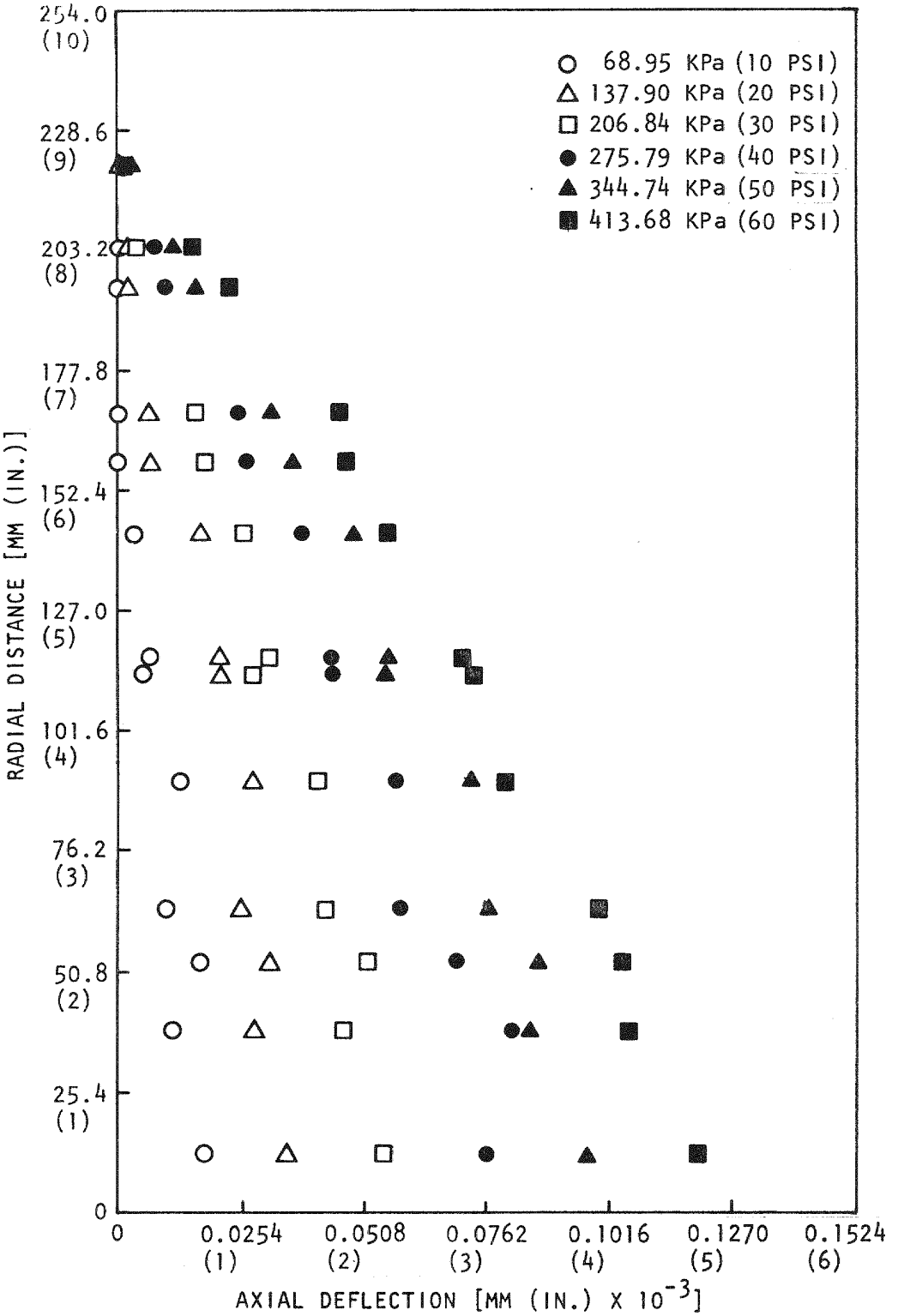

Fig. 11. Axial displacement vs radial distance of grid plate, average values for loading and unloading cases

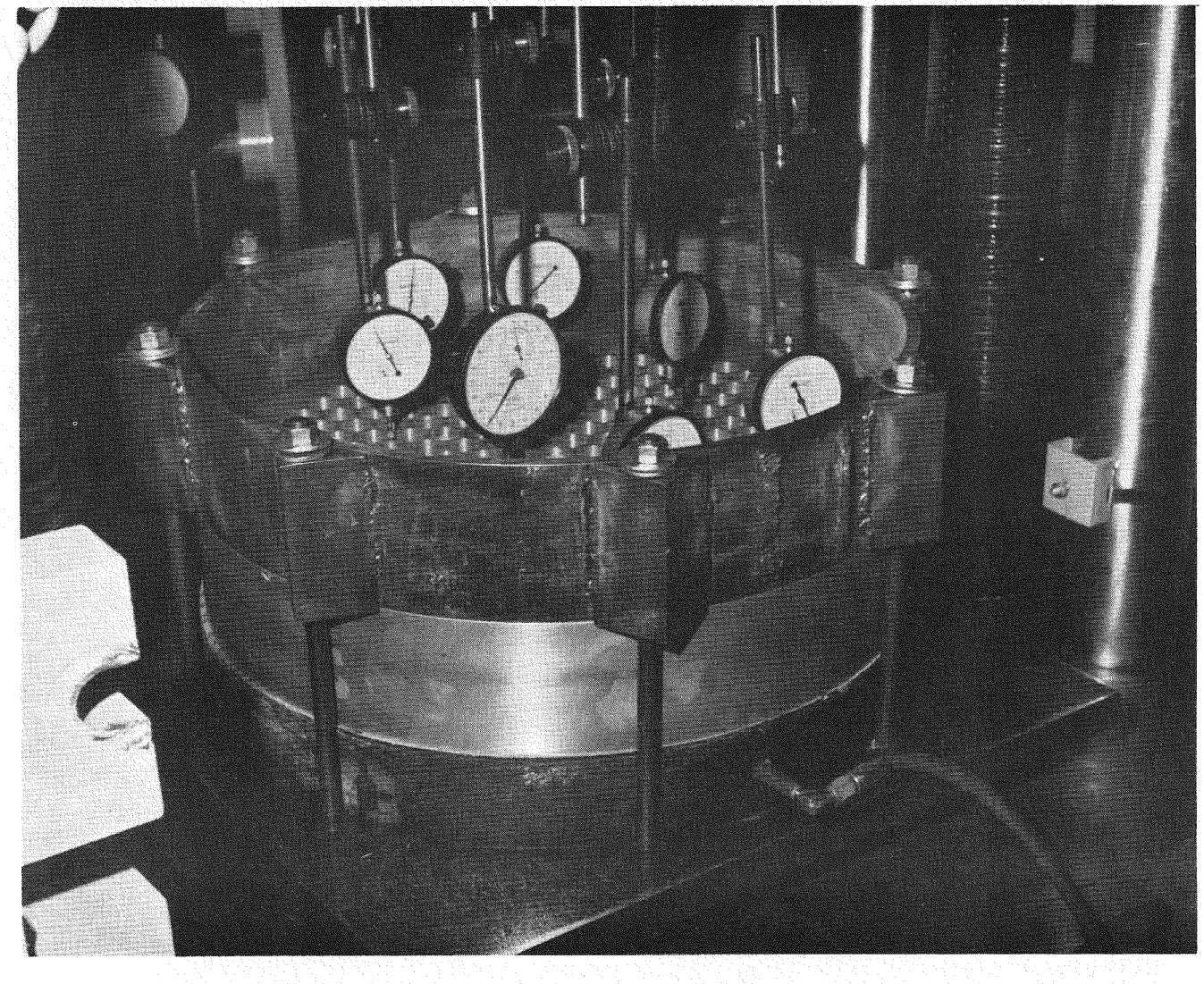

Fig. 12. Axial deflection test arrangement

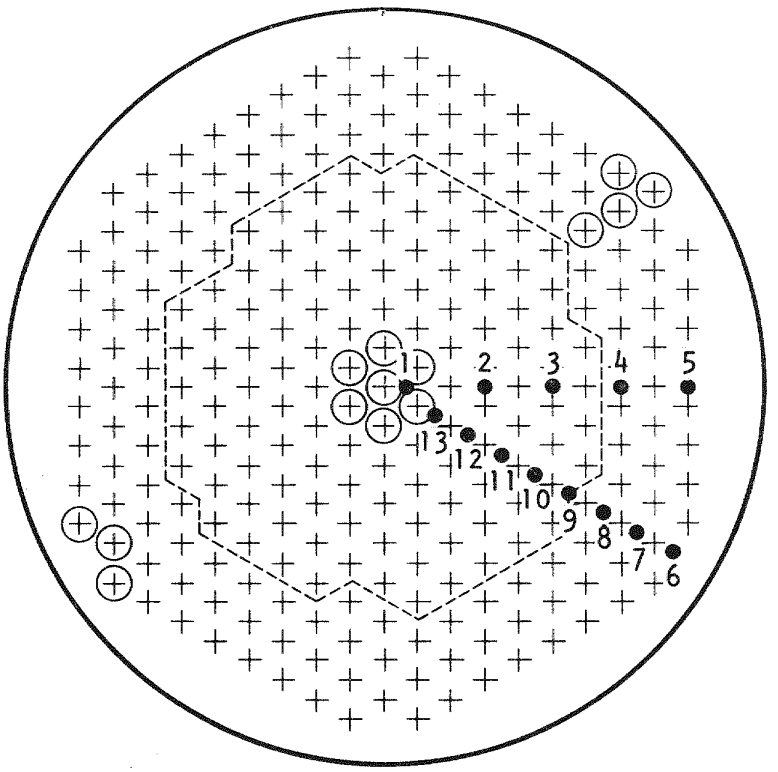

Fig. 13. Test axial deflection measuring point locations

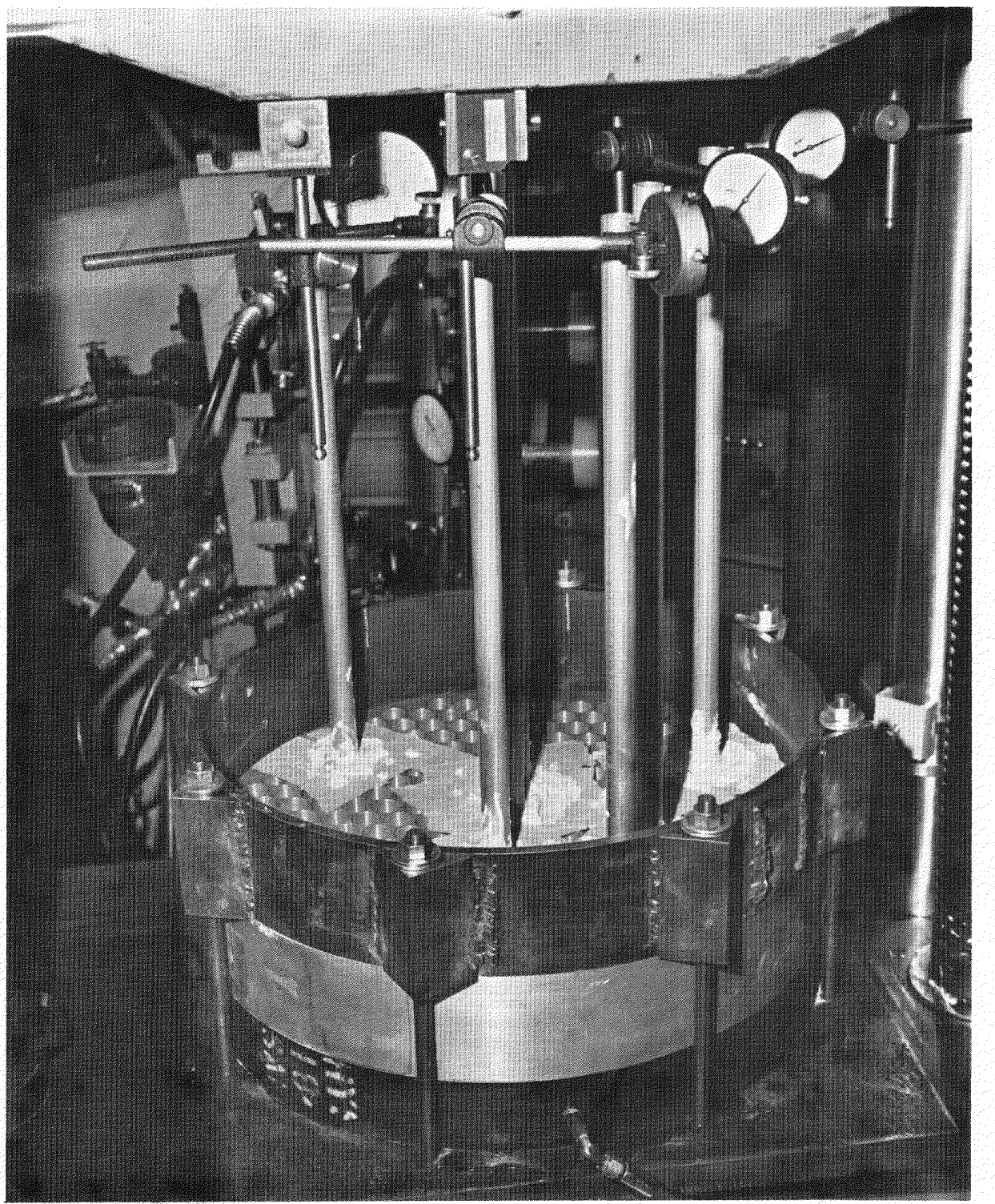

Fig. 14. Radial tip deflection test arrangement

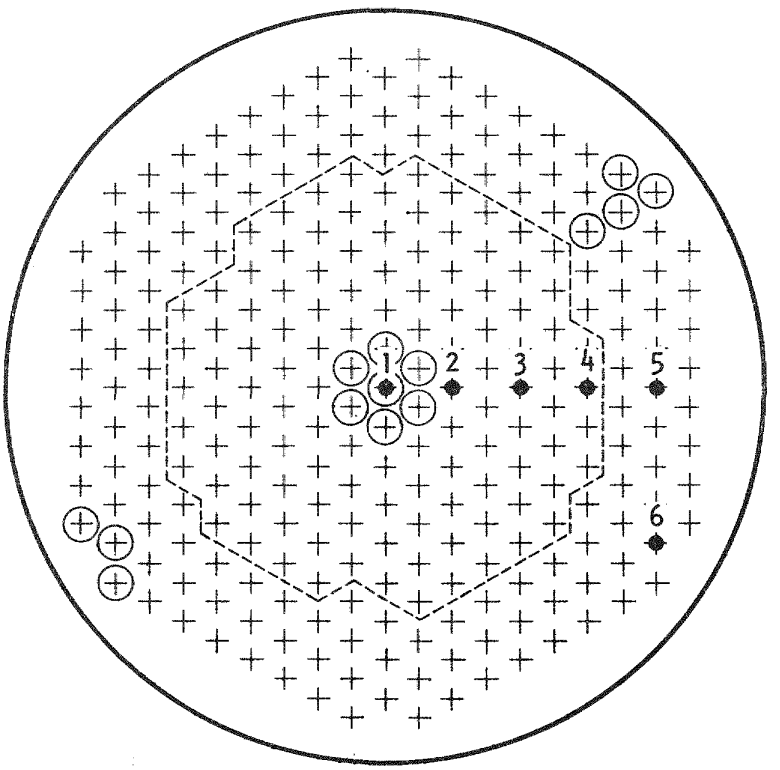

Fig. 15. Test radial deflection measuring point locations

cycled twice (from low pressure to high pressure to low pressure). Data for grid plate deflection are given in Table 6, and data for tube displacements are presented in Table 7. Tables 8 through 10 present axial displacement readings during loading and unloading. The tubes were fixed in the grid plate model using plaster of paris.

TABLE 6
AXIAL DISPLACEMENT READINGS ON GRID PLATE MODEL[a]

Pressure [kPa (psi)]	Axial Displacement [mm (10^{-3} in.)]												
	Point												
	1	2	3	4	5	6	7	8	9	10	11	12	13
0	0	0	0	0	0	0	0	0	0	0	0	0	0
68.95 (10)	0.015 (0.6)	0.013 (0.5)	0.003 (0.1)	0	-0.003 (-0.1)	0	0	0	0	0	0.013 (0.5)	0.005 (0.2)	0.005 (0.2)
137.90 (20)	0.030 (1.2)	0.025 (1.0)	0.020 (0.8)	0.005 (0.2)	-0.003 (-0.1)	0.003 (0.1)	0	0	0.015 (0.6)	0.018 (0.7)	0.023 (0.9)	0.023 (0.9)	0.020 (0.8)
206.84 (30)	0.051 (2.0)	0.048 (1.9)	0.025 (1.0)	0.015 (0.6)	-0.003 (-0.1)	0.003 (0.1)	0	0.008 (0.3)	0.025 (1.0)	0.025 (1.0)	0.038 (1.5)	0.033 (1.3)	0.041 (1.6)
275.79 (40)	0.071 (2.8)	0.066 (2.6)	0.041 (1.6)	0.025 (1.0)	0	0.003 (0.1)	0.003 (0.1)	0.023 (0.9)	0.033 (1.3)	0.036 (1.4)	0.051 (2.0)	0.051 (2.0)	0.058 (2.3)
344.74 (50)	0.094 (3.7)	0.081 (3.2)	0.053 (2.1)	0.036 (1.4)	0.005 (0.2)	0.003 (0.1)	0.010 (0.4)	0.028 (1.1)	0.048 (1.9)	0.051 (2.0)	0.064 (2.5)	0.076 (3.0)	0.081 (3.2)
413.68 (60)	0.119 (4.7)	0.104 (4.1)	0.074 (2.9)	0.048 (1.9)	0.013 (0.5)	0.003 (0.1)	0.020 (0.8)	0.043 (1.7)	0.056 (2.2)	0.071 (2.8)	0.089 (3.5)	0.102 (4.0)	0.104 (4.1)
344.74 (50)	0.102 (4.0)	0.094 (3.7)	0.061 (2.4)	0.041 (1.6)	0.013 (0.5)	0.003 (0.1)	0.010 (0.4)	0.033 (1.3)	0.051 (2.0)	0.064 (2.5)	0.076 (3.0)	0.079 (3.1)	0.086 (3.4)
275.79 (40)	0.081 (3.2)	0.076 (3.0)	0.051 (2.0)	0.028 (1.1)	0.010 (0.4)	0.003 (0.1)	0.005 (0.2)	0.025 (1.0)	0.046 (1.8)	0.051 (2.0)	0.064 (2.5)	0.064 (2.5)	0.069 (2.7)
206.84 (30)	0.061 (2.4)	0.056 (2.2)	0.033 (1.3)	0.023 (0.9)	0.005 (0.2)	0.003 (0.1)	0.003 (0.1)	0.023 (0.9)	0.030 (1.2)	0.036 (1.4)	0.038 (1.5)	0.051 (2.0)	0.048 (1.9)
137.90 (20)	0.038 (1.5)	0.038 (1.5)	0.023 (0.9)	0.013 (0.5)	0.003 (0.1)	0.003 (0.1)	0	0.010 (0.4)	0.023 (0.9)	0.028 (1.1)	0.025 (1.0)	0.028 (1.1)	0.030 (1.2)
68.95 (10)	0.020 (0.8)	0.020 (0.8)	0.008 (0.3)	0	-0.003 (-0.1)	0.003 (0.1)	0	0	0.008 (0.3)	0.010 (0.4)	0.013 (0.5)	0.015 (0.6)	0.013 (0.5)

TABLE 6 (Continued)

Pressure [kPa (psi)]	Axial Displacement [mm (10^{-3} in.)]												
	Point												
	1	2	3	4	5	6	7	8	9	10	11	12	13
0	0.003 (0.1)	0	0	0	-0.005 (-0.2)	0.003 (0.1)	0	-0.003 (-0.1)	0	0	0	0	-0.005 (-0.2)
0	0	0	0	0	0	0	0	0	0	0	0	0	0
68.95 (10)	0.015 (0.6)	0.015 (0.6)	0.005 (0.2)	0	0	0	0	0	0	0.003 (0.1)	0.013 (0.5)	0.005 (0.2)	0.010 (0.4)
137.90 (20)	0.030 (1.2)	0.025 (1.0)	0.020 (0.8)	0.003 (0.1)	0	0	0.003 (0.1)	0.003 (0.1)	0.008 (0.3)	0.010 (0.4)	0.025 (1.0)	0.023 (0.9)	0.028 (1.1)
206.84 (30)	0.048 (1.9)	0.048 (1.9)	0.025 (1.0)	0.013 (0.5)	0	0	0.005 (0.2)	0.010 (0.4)	0.020 (0.8)	0.025 (1.0)	0.038 (1.5)	0.036 (1.4)	0.043 (1.7)
275.79 (40)	0.069 (2.7)	0.064 (2.5)	0.038 (1.5)	0.023 (0.9)	0.005 (0.2)	0	0.013 (0.5)	0.023 (0.9)	0.030 (1.2)	0.038 (1.5)	0.051 (2.0)	0.053 (2.1)	0.064 (2.5)
344.74 (50)	0.094 (3.7)	0.081 (3.2)	0.051 (2.0)	0.030 (1.2)	0.010 (0.4)	0	0.020 (0.8)	0.030 (1.2)	0.046 (1.8)	0.051 (2.0)	0.076 (3.0)	0.076 (3.0)	0.084 (3.3)
413.68 (60)	0.119 (4.7)	0.104 (4.1)	0.074 (2.9)	0.046 (1.8)	0.018 (0.7)	0	0.025 (1.0)	0.048 (1.9)	0.056 (2.2)	0.071 (2.8)	0.089 (3.5)	0.097 (3.8)	0.107 (4.2)
344.74 (50)	0.099 (3.9)	0.091 (3.6)	0.056 (2.2)	0.038 (1.5)	0.018 (0.7)	0	0.023 (0.9)	0.036 (1.4)	0.051 (2.0)	0.058 (2.3)	0.076 (3.0)	0.076 (3.0)	0.089 (3.5)
275.79 (40)	0.081 (3.2)	0.074 (2.9)	0.046 (1.8)	0.028 (1.1)	0.015 (0.6)	0	0.018 (0.7)	0.028 (1.1)	0.043 (1.7)	0.051 (2.0)	0.064 (2.5)	0.064 (2.5)	0.071 (2.8)
206.84 (30)	0.058 (2.3)	0.053 (2.1)	0.028 (1.1)	0.020 (0.8)	0.010 (0.4)	0	0.010 (0.4)	0.023 (0.9)	0.028 (1.1)	0.038 (1.5)	0.051 (2.0)	0.051 (2.0)	0.053 (2.1)

TABLE 6 (Continued)

Pressure [kPa (psi)]	Axial Displacement [mm (10^{-3} in.)]												
	Point												
	1	2	3	4	5	6	7	8	9	10	11	12	13
137.90 (20)	0.038 (1.5)	0.036 (1.4)	0.020 (0.8)	0.008 (0.3)	0.008 (0.3)	0	0.003 (0.1)	0.013 (0.5)	0.023 (0.9)	0.028 (1.1)	0.038 (1.5)	0.028 (1.1)	0.033 (1.3)
68.95 (10)	0.018 (0.7)	0.018 (0.7)	0.005 (0.2)	0	0.003 (0.1)	0	0	0	0.005 (0.2)	0.013 (0.5)	0.013 (0.5)	0.013 (0.5)	0.015 (0.6)
0	0	0	0	0	0	0	0	0	0	0	0	0	-0.003 (-0.1)

(a) Data taken on January 9, 1976; point locations shown in Fig. 10. Torque on test fixture bolt nuts = 67.791 N·m (50 ft-lb). Dial indicator gauge on points 1 and 5 have divisions of ten thousandths [0.00254 mm (0.0001 in.)]; all others, thousandths [0.0254 mm (0.001 in.)]. Readings are given in mils [0.0254 mm (0.001 in.)].

TABLE 7
RADIAL DISPLACEMENT READINGS ON THE TIPS OF THE TUBES ATTACHED TO GRID PLATE MODEL[a]

Pressure [kPa (psi)]	Displacement [mm (10^{-3} in.)]					
	Tube					
	1	2	3	4	5	6
0	0	0	0	0	0	0
68.95 (10)	0	0.003 (0.1)	0.025 (1.0)	0.046 (1.8)	0.046 (1.8)	0.033 (1.3)
137.90 (20)	0	0.043 (1.7)	0.066 (2.6)	0.099 (3.9)	0.117 (4.6)	0.081 (3.2)
206.84 (30)	0	0.079 (3.1)	0.104 (4.1)	0.162 (6.4)	0.201 (7.9)	0.135 (5.3)
275.79 (40)	0.003 (0.1)	0.122 (4.8)	0.147 (5.8)	0.229 (9.0)	0.279 (11.0)	0.185 (7.3)
344.74 (50)	0.013 (0.5)	0.155 (6.1)	0.180 (7.1)	0.295 (11.6)	0.371 (14.6)	0.236 (9.3)
413.68 (60)	0.023 (0.9)	0.208 (8.2)	0.221 (8.7)	0.356 (14.0)	0.460 (18.1)	0.294 (11.6)
344.74 (50)	0.033 (1.3)	0.203 (8.0)	0.191 (7.5)	0.320 (12.6)	0.411 (16.2)	0.257 (10.1)
275.79 (40)	0.033 (1.3)	0.185 (7.3)	0.152 (6.0)	0.254 (10.0)	0.335 (13.2)	0.203 (8.0)
206.84 (30)	0.033 (1.3)[b]	0.140 (5.5)	0.109 (4.3)	0.198 (7.8)	0.257 (10.1)	0.152 (6.0)
137.90 (20)	0.030 (1.2)	0.104 (4.1)	0.076 (3.0)	0.132 (5.2)	0.178 (7.0)	0.102 (4.0)
68.95 (10)	0.030 (1.2)	0.064 (2.5)	0.033 (1.3)	0.069 (2.7)	0.097 (3.8)	0.051 (2.0)
0	0.023 (0.9)	0.028 (1.1)	0	0.003 (0.1)	0.023 (0.9)	0
0	0	0	0	0	0	0
68.95 (10)	0	0	0.020 (0.8)	0.038 (1.5)	0.038 (1.5)	0.028 (1.1)
137.90 (20)	0	0.028 (1.1)	0.061 (2.4)	0.104 (4.1)	0.117 (4.6)	0.089 (3.5)
206.84 (30)	0	0.069 (2.7)	0.102 (4.0)	0.168 (6.6)	0.196 (7.7)	0.142 (5.6)
275.79 (40)	0	0.107 (4.2)	0.147 (5.8)	0.231 (9.1)	0.277 (10.9)	0.198 (7.8)

TABLE 7 (Continued)

Pressure [kPa (psi)]	Displacement [mm (10^{-3} in.)]					
	Tube					
	1	2	3	4	5	6
344.74 (50)	0.003 (0.1)	0.150 (5.9)	0.178 (7.0)	0.297 (11.7)	0.361 (14.2)	0.246 (9.7)
413.68 (60)	0.013 (0.5)	0.208 (8.2)[c]	0.216 (8.5)	0.356 (14.0)	0.452 (17.8)	0.300 (11.8)
344.74 (50)	0.018 (0.7)	0.183 (7.2)	0.183 (7.2)	0.312 (12.3)	0.394 (15.5)	0.257 (10.1)
275.79 (40)	0.018 (0.7)	0.165 (6.5)	0.147 (5.8)	0.254 (10.0)	0.320 (12.6)	0.206 (8.1)
206.84 (30)	0.018 (0.7)	0.127 (5.0)	0.107 (4.2)	0.193 (7.6)	0.236 (9.3)	0.155 (6.1)
137.90 (20)	0.018 (0.7)	0.089 (3.5)	0.071 (2.8)	0.130 (5.1)	0.155 (6.1)	0.102 (4.0)
68.95 (10)	0.015 (0.6)	0.038 (1.5)	0.028 (1.1)	0.064 (2.5)	0.076 (3.0)	0.051 (2.0)
0	0.013 (0.5)	0.013 (0.5)	0	0.003 (0.1)	0.003 (0.1)	0

[a] Data taken on January 29, 1976; tube location shown in Fig. 12. Torque on test fixture bolt nuts = 67.791 N·m (50 ft-lb). Dial indicator gauge on tube 1 has divisions of 0.00254 mm (0.0001 in.); all others, 0.0254 mm (0.001 in.). Readings are given in mils [0.0254 mm (0.001 in.)] and are radial outward from center of plate.

[b] Gauge stuck.

[c] Questionable reading.

TABLE 8
AXIAL DISPLACEMENT OF THE GRID PLATE MODEL DURING LOADING

Pressure [kPa (psi)]	Axial Displacement [mm (10^{-3} in.)]												
	Point												
	1	2	3	4	5	6	7	8	9	10	11	12	13
0	0	0	0	0	0	0	0	0	0	0	0	0	0
	0	0	0	0	0	0	0	0	0	0	0	0	0
Average	0	0	0	0	0	0	0	0	0	0	0	0	0
68.95 (10)	0.015 (0.6)	0.013 (0.5)	0.003 (0.1)	0	0.003 (0.1)	0	0	0	0	0	0.013 (0.5)	0.005 (0.2)	0.005 (0.2)
	0.015 (0.6)	0.015 (0.6)	0.005 (0.2)	0	0	0	0	0	0	0.003 (0.1)	0.013 (0.5)	0.005 (0.2)	0.010 (0.4)
Average	0.015 (0.6)	0.014 (0.55)	0.004 (0.15)	0	0.001 (0.05)	0	0	0	0	0.001 (0.05)	0.013 (0.5)	0.005 (0.2)	0.008 (0.3)
137.90 (20)	0.030 (1.2)	0.025 (1.0)	0.020 (0.8)	0.005 (0.2)	0.003 (0.1)	0.003 (0.1)	0	0	0.015 (0.6)	0.018 (0.7)	0.023 (0.9)	0.023 (0.9)	0.020 (0.8)
	0.030 (1.2)	0.025 (1.0)	0.020 (0.8)	0.003 (0.1)	0	0	0.003 (0.1)	0.003 (0.1)	0.008 (0.3)	0.010 (0.4)	0.025 (1.0)	0.023 (0.9)	0.028 (1.1)
Average	0.030 (1.2)	0.025 (1.0)	0.020 (0.8)	0.004 (0.15)	0.001 (0.05)	0.001 (0.05)	0.001 (0.05)	0.001 (0.05)	0.011 (0.45)	0.014 (0.55)	0.024 (0.95)	0.023 (0.9)	0.024 (0.95)
206.84 (30)	0.051 (2.0)	0.048 (1.9)	0.025 (1.0)	0.015 (0.6)	0.003 (0.1)	0.003 (0.1)	0	0.008 (0.3)	0.025 (1.0)	0.025 (1.0)	0.038 (1.5)	0.033 (1.3)	0.041 (1.6)
	0.048 (1.9)	0.048 (1.9)	0.025 (1.0)	0.013 (0.5)	0	0	0.005 (0.2)	0.010 (0.4)	0.020 (0.8)	0.025 (1.0)	0.038 (1.5)	0.036 (1.4)	0.043 (1.7)
Average	0.050 (1.95)	0.048 (1.9)	0.025 (1.0)	0.014 (0.55)	0.001 (0.05)	0.001 (0.05)	0.003 (0.1)	0.009 (0.35)	0.023 (0.9)	0.025 (1.0)	0.038 (1.5)	0.034 (1.35)	0.042 (1.65)

TABLE 8 (Continued)

Pressure [kPa (psi)]	Axial Displacement [mm (10^{-3} in.)]												
	Point												
	1	2	3	4	5	6	7	8	9	10	11	12	13
275.79 (40)	0.071 (2.8)	0.066 (2.6)	0.041 (1.6)	0.025 (1.0)	0	0.003 (0.1)	0.003 (0.1)	0.023 (0.9)	0.033 (1.3)	0.036 (1.4)	0.051 (2.0)	0.051 (2.0)	0.058 (2.3)
	0.069 (2.7)	0.064 (2.5)	0.038 (1.5)	0.023 (0.9)	0.005 (0.2)	0	0.013 (0.5)	0.023 (0.9)	0.030 (1.2)	0.038 (1.5)	0.051 (2.0)	0.053 (2.1)	0.064 (2.5)
Average	0.070 (2.75)	0.065 (2.55)	0.039 (1.55)	0.024 (0.95)	0.003 (0.1)	0.001 (0.05)	0.008 (0.3)	0.023 (0.9)	0.031 (1.25)	0.037 (1.45)	0.051 (2.0)	0.052 (2.05)	0.061 (2.4)
344.74 (50)	0.094 (3.7)	0.081 (3.2)	0.053 (2.1)	0.036 (1.4)	0.005 (0.2)	0.003 (0.1)	0.010 (0.4)	0.028 (1.1)	0.049 (1.9)	0.051 (2.0)	0.064 (2.5)	0.076 (3.0)	0.081 (3.2)
	0.094 (3.7)	0.081 (3.2)	0.051 (2.0)	0.030 (1.2)	0.010 (0.4)	0	0.020 (0.8)	0.030 (1.2)	0.046 (1.8)	0.051 (2.0)	0.076 (3.0)	0.076 (3.0)	0.084 (3.3)
Average	0.094 (3.7)	0.081 (3.2)	0.052 (2.05)	0.033 (1.3)	0.008 (0.3)	0.001 (0.05)	0.015 (0.6)	0.029 (1.15)	0.047 (1.85)	0.051 (2.0)	0.070 (2.75)	0.076 (3.0)	0.083 (3.25)
413.68 (60)	0.119 (4.7)	0.104 (4.1)	0.074 (2.9)	0.048 (1.9)	0.013 (0.5)	0.003 (0.1)	0.020 (0.8)	0.043 (1.7)	0.056 (2.2)	0.071 (2.8)	0.089 (3.5)	0.102 (4.0)	0.104 (4.1)
	0.119 (4.7)	0.104 (4.1)	0.074 (2.9)	0.046 (1.8)	0.018 (0.7)	0	0.025 (1.0)	0.048 (1.9)	0.056 (2.2)	0.071 (2.8)	0.089 (3.5)	0.097 (3.8)	0.107 (4.2)
Average	0.119 (4.7)	0.104 (4.1)	0.074 (2.9)	0.047 (1.85)	0.015 (0.6)	0.001 (0.05)	0.023 (0.9)	0.046 (1.8)	0.056 (2.2)	0.071 (2.8)	0.089 (3.5)	0.099 (3.9)	0.105 (4.15)

TABLE 9
AXIAL DISPLACEMENT OF THE GRID PLATE MODEL DURING UNLOADING

Pressure [kPa (psi)]	Axial Displacement [mm (10^{-3} in.)]												
	Point												
	1	2	3	4	5	6	7	8	9	10	11	12	13
413.68 (60)	0.119 (4.7)	0.104 (4.1)	0.074 (2.9)	0.048 (1.9)	0.013 (0.5)	0.003 (0.1)	0.020 (0.8)	0.043 (1.7)	0.056 (2.2)	0.071 (2.8)	0.089 (3.5)	0.102 (4.0)	0.104 (4.1)
	0.119 (4.7)	0.104 (4.1)	0.074 (2.9)	0.046 (1.8)	0.018 (0.7)	0	0.025 (1.0)	0.048 (1.9)	0.056 (2.2)	0.071 (2.8)	0.089 (3.5)	0.097 (3.8)	0.107 (4.2)
Average	0.119 (4.7)	0.104 (4.1)	0.074 (2.9)	0.047 (1.85)	0.015 (0.6)	0.001 (0.05)	0.023 (0.9)	0.046 (1.8)	0.056 (2.2)	0.071 (2.8)	0.089 (3.5)	0.099 (3.9)	0.105 (4.15)
344.74 (50)	0.102 (4.0)	0.094 (3.7)	0.061 (2.4)	0.041 (1.6)	0.013 (0.5)	0.003 (0.1)	0.010 (0.4)	0.033 (1.3)	0.051 (2.0)	0.064 (2.5)	0.076 (3.0)	0.079 (3.1)	0.086 (3.4)
	0.099 (3.9)	0.091 (3.6)	0.056 (2.2)	0.038 (1.5)	0.018 (0.7)	0	0.023 (0.9)	0.035 (1.4)	0.051 (2.0)	0.058 (2.3)	0.076 (3.0)	0.076 (3.0)	0.089 (3.5)
Average	0.100 (3.95)	0.093 (3.65)	0.058 (2.3)	0.039 (1.55)	0.015 (0.6)	0.001 (0.05)	0.017 (0.65)	0.034 (1.35)	0.051 (2.0)	0.061 (2.4)	0.076 (3.0)	0.077 (3.05)	0.088 (3.45)
275.79 (40)	0.081 (3.2)	0.076 (3.0)	0.051 (2.0)	0.028 (1.1)	0.010 (0.4)	0.003 (0.1)	0.005 (0.2)	0.025 (1.0)	0.046 (1.8)	0.051 (2.0)	0.064 (2.5)	0.064 (2.5)	0.069 (2.7)
	0.081 (3.2)	0.074 (2.9)	0.046 (1.8)	0.028 (1.1)	0.015 (0.6)	0	0.018 (0.7)	0.028 (1.1)	0.043 (1.7)	0.051 (2.0)	0.064 (2.5)	0.064 (2.5)	0.071 (2.8)
Average	0.081 (3.2)	0.075 (2.95)	0.048 (1.9)	0.028 (1.1)	0.013 (0.5)	0.001 (0.05)	0.011 (0.45)	0.027 (1.05)	0.044 (1.75)	0.051 (2.0)	0.064 (2.5)	0.064 (2.5)	0.070 (2.75)

TABLE 9 (Continued)

Pressure [kPa (psi)]	Axial Displacement [mm (10^{-3} in.)]												
	Point												
	1	2	3	4	5	6	7	8	9	10	11	12	13
206.84 (30)	0.061 (2.4)	0.056 (2.2)	0.033 (1.3)	0.023 (0.9)	0.005 (0.2)	0.003 (0.1)	0.003 (0.1)	0.023 (0.9)	0.030 (1.2)	0.036 (1.4)	0.038 (1.5)	0.051 (2.0)	0.048 (1.9)
	0.058 (2.3)	0.053 (2.1)	0.028 (1.1)	0.020 (0.8)	0.010 (0.4)	0	0.010 (0.4)	0.023 (0.9)	0.028 (1.1)	0.038 (1.5)	0.051 (2.0)	0.051 (2.0)	0.053 (2.1)
Average	0.060 (2.35)	0.055 (2.15)	0.030 (1.2)	0.022 (0.85)	0.008 (0.3)	0.001 (0.05)	0.006 (0.25)	0.023 (0.9)	0.029 (1.15)	0.037 (1.45)	0.044 (1.75)	0.051 (2.0)	0.051 (2.0)
137.90 (20)	0.038 (1.5)	0.038 (1.5)	0.023 (0.9)	0.013 (0.5)	0.003 (0.1)	0.003 (0.1)	0	0.010 (0.4)	0.023 (0.9)	0.028 (1.1)	0.025 (1.0)	0.028 (1.1)	0.030 (1.2)
	0.038 (1.5)	0.035 (1.4)	0.020 (0.8)	0.008 (0.3)	0.008 (0.3)	0	0.003 (0.1)	0.013 (0.5)	0.023 (0.9)	0.028 (1.1)	0.038 (1.5)	0.028 (1.1)	0.033 (1.3)
Average	0.038 (1.5)	0.037 (1.45)	0.022 (0.85)	0.010 (0.4)	0.005 (0.2)	0.001 (0.05)	0.001 (0.05)	0.011 (0.45)	0.023 (0.9)	0.028 (1.1)	0.032 (1.25)	0.028 (1.1)	0.032 (1.25)
68.95 (10)	0.020 (0.8)	0.020 (0.8)	0.008 (0.3)	0	-0.003 (-0.1)	0.003 (0.1)	0	0	0.008 (0.3)	0.010 (0.4)	0.013 (0.5)	0.015 (0.6)	0.013 (0.5)
	0.018 (0.7)	0.018 (0.7)	0.005 (0.2)	0	0.003 (0.1)	0	0	0	0.005 (0.2)	0.013 (0.5)	0.013 (0.5)	0.013 (0.5)	0.015 (0.6)
Average	0.019 (0.75	0.019 (0.75)	0.006 (0.25)	0	0	0.001 (0.05)	0	0	0.006 (0.25)	0.011 (0.45)	0.013 (0.5)	0.014 (0.55)	0.014 (0.55)

TABLE 9 (Continued)

Pressure [kPa (psi)]	Axial Displacement [mm (10^{-3} in.)]												
	Point												
	1	2	3	4	5	6	7	8	9	10	11	12	13
0	0.003 (0.1)	0	0	0	-0.005 (-0.2)	0.003 (0.1)	0	-0.003 (-0.1)	0	0	0	0	-0.005 (-0.2)
	0	0	0	0	0	0	0	0	0	0	0	0	-0.003 (-0.1)
Average	0.001 (0.05)	0	0	0	-0.003 (-0.1)	0.001 (0.05)	0	-0.001 (-0.05)	0	0	0	0	-0.004 (-0.15)

TABLE 10
AVERAGE AXIAL DISPLACEMENT OF THE GRID PLATE MODEL DURING LOADING AND UNLOADING

Pressure [kPa (psi)]	Axial Displacement [mm (10^{-3} in.)]												
	Point												
	1	2	3	4	5	6	7	8	9	10	11	12	13
0	0	0	0	0	0	0	0	0	0	0	0	0	0
	0.003 (0.1)	0	0	0	-0.005 (-0.2)	0.003 (0.1)	0	-0.003 (-0.1)	0	0	0	0	-0.005 (-0.2)
	0	0	0	0	0	0	0	0	0	0	0	0	0
	0	0	0	0	0	0	0	0	0	0	0	0	-0.003 (-0.1)
Average	0.001 (0.025)	0	0	0	-0.001 (-0.05)	0.001 (0.025	0	-0.001 (-0.025)	0	0	0	0	-0.002 (-0.075)
68.95 (10)	0.015 (0.6)	0.013 (0.5)	0.003 (0.1)	0	-0.003 (-0.1)	0	0	0	0	0	0.013 (0.5)	0.005 (0.2)	0.005 (0.2)
	0.020 (0.8)	0.020 (0.8)	0.008 (0.3)	0	-0.003 (-0.1)	0.003 (0.1)	0	0	0.008 (0.3)	0.010 (0.4)	0.013 (0.5)	0.015 (0.6)	0.013 (0.5)
	0.015 (0.6)	0.015 (0.6)	0.005 (0.2)	0	0	0	0	0	0	0.003 (0.1)	0.013 (0.5)	0.005 (0.2)	0.010 (0.4)
	0.018 (0.7)	0.018 (0.7)	0.005 (0.2)	0	0.003 (0.1)	0	0	0	0.005 (0.2)	0.013 (0.5)	0.013 (0.5)	0.013 (0.5)	0.015 (0.6)
Average	0.017 (0.675)	0.017 (0.65)	0.005 (0.2)	0	-0.001 (-0.025)	0.001 (0.025)	0	0	0.003 (0.125)	0.006 (0.25)	0.013 (0.5)	0.010 (0.375)	0.011 (0.425)
137.90 (20)	0.030 (1.2)	0.025 (1.0)	0.020 (0.8)	0.005 (0.2)	-0.003 (-0.1)	0.003 (0.1)	0	0	0.015 (0.6)	0.018 (0.7)	0.023 (0.9)	0.023 (0.9)	0.020 (0.8)
	0.038 (1.5)	0.038 (1.5)	0.023 (0.9)	0.013 (0.5)	0.003 (0.1)	0.003 (0.1)	0	0.010 (0.4)	0.023 (0.9)	0.028 (1.1)	0.025 (1.0)	0.028 (1.1)	0.030 (1.2)
	0.030 (1.2)	0.025 (1.0)	0.020 (0.8)	0.003 (0.1)	0	0	0.003 (0.1)	0.003 (0.1)	0.008 (0.3)	0.010 (0.4)	0.025 (1.0)	0.023 (0.9)	0.028 (1.1)
	0.038 (1.5)	0.036 (1.4)	0.020 (0.8)	0.008 (0.3)	0.008 (0.3)	0	0.003 (0.1)	0.013 (0.5)	0.023 (0.9)	0.028 (1.1)	0.038 (1.5)	0.028 (1.1)	0.033 (1.3)
Average	0.034 (1.35)	0.031 (1.225)	0.021 (0.825)	0.007 (0.275)	0.002 (0.075	0.001 (0.05)	0.001 (0.05)	0.006 (0.25)	0.017 (0.675)	0.021 (0.825)	0.028 (1.1)	0.025 (1.0)	0.028 (1.1)
206.84 (30)	0.051 (2.0)	0.048 (1.9)	0.025 (1.0)	0.015 (0.6)	-0.003 (-0.1)	0.003 (0.1)	0	0.008 (0.3)	0.025 (1.0)	0.025 (1.0)	0.038 (1.5)	0.033 (1.3)	0.041 (1.6)
	0.061 (2.4)	0.056 (2.2)	0.033 (1.3)	0.023 (0.9)	0.005 (0.2)	0.003 (0.1)	0.003 (0.1)	0.023 (0.9)	0.030 (1.2)	0.036 (1.4)	0.038 (1.5)	0.051 (2.0)	0.048 (1.9)
	0.048 (1.9)	0.048 (1.9)	0.025 (1.0)	0.013 (0.5)	0	0	0.005 (0.2)	0.010 (0.4)	0.020 (0.8)	0.025 (1.0)	0.038 (1.5)	0.036 (1.4)	0.043 (1.7)
	0.058 (2.3)	0.053 (2.1)	0.028 (1.1)	0.020 (0.8)	0.010 (0.4)	0	0.010 (0.4)	0.023 (0.9)	0.028 (1.1)	0.038 (1.5)	0.051 (2.0)	0.051 (2.0)	0.053 (2.1)
Average	0.055 (2.15)	0.051 (2.025)	0.028 (1.1)	0.018 (0.7)	0.003 (0.125)	0.001 (0.05)	0.004 (0.175)	0.016 (0.625)	0.026 (1.025)	0.031 (1.225)	0.041 (1.625)	0.043 (1.675)	0.048 (1.875)

TABLE 10 (Continued)

Pressure [kPa (psi)]	Axial Displacement [mm (10^{-3} in.)]												
	Point												
	1	2	3	4	5	6	7	8	9	10	11	12	13
275.79 (40)	0.071 (2.8)	0.066 (2.6)	0.041 (1.6)	0.025 (1.0)	0	0.003 (0.1)	0.003 (0.1)	0.023 (0.9)	0.033 (1.3)	0.036 (1.4)	0.051 (2.0)	0.051 (2.0)	0.058 (2.3)
	0.081 (3.2)	0.076 (3.0)	0.051 (2.0)	0.028 (1.1)	0.010 (0.4)	0.003 (0.1)	0.005 (0.2)	0.025 (1.0)	0.046 (1.8)	0.051 (2.0)	0.064 (2.5)	0.064 (2.5)	0.069 (2.7)
	0.069 (2.7)	0.064 (2.5)	0.038 (1.5)	0.023 (0.9)	0.005 (0.2)	0	0.013 (0.5)	0.023 (0.9)	0.030 (1.2)	0.038 (1.5)	0.051 (2.0)	0.053 (2.1)	0.064 (2.5)
	0.081 (3.2)	0.074 (2.9)	0.046 (1.8)	0.028 (1.1)	0.015 (0.6)	0	0.018 (0.7)	0.028 (1.1)	0.043 (1.7)	0.051 (2.0)	0.064 (2.5)	0.064 (2.5)	0.071 (2.8)
Average	0.076 (2.975)	0.070 (2.75)	0.044 (1.725)	0.026 (1.025)	0.008 (0.3)	0.001 (0.05)	0.010 (0.375)	0.025 (0.975)	0.038 (1.5)	0.044 (1.725)	0.057 (2.25)	0.058 (2.275)	0.081 (3.2)
344.74 (50)	0.094 (3.7)	0.081 (3.2)	0.053 (2.1)	0.036 (1.4)	0.005 (0.2)	0.003 (0.1)	0.010 (0.4)	0.028 (1.1)	0.048 (1.9)	0.051 (2.0)	0.064 (2.5)	0.076 (3.0)	0.081 (3.2)
	0.102 (4.0)	0.094 (3.7)	0.061 (2.4)	0.041 (1.6)	0.013 (0.5)	0.003 (0.1)	0.010 (0.4)	0.033 (1.3)	0.051 (2.0)	0.064 (2.5)	0.076 (3.0)	0.079 (3.1)	0.086 (3.4)
	0.094 (3.7)	0.081 (3.2)	0.051 (2.0)	0.030 (1.2)	0.010 (0.4)	0	0.020 (0.8)	0.030 (1.2)	0.046 (1.8)	0.051 (2.0)	0.076 (3.0)	0.076 (3.0)	0.084 (3.3)
	0.099 (3.9)	0.091 (3.6)	0.056 (2.2)	0.038 (1.5)	0.018 (0.7)	0	0.023 (0.9)	0.036 (1.4)	0.051 (2.0)	0.058 (2.3)	0.076 (3.0)	0.076 (3.0)	0.089 (3.5)
Average	0.097 (3.825)	0.087 (3.425)	0.055 (2.175)	0.036 (1.425)	0.011 (0.45)	0.001 (0.05)	0.016 (0.625)	0.032 (1.25)	0.049 (1.925)	0.056 (2.2)	0.073 (2.875)	0.077 (3.025)	0.085 (3.35)
413.68 (60)	0.119 (4.7)	0.104 (4.1)	0.074 (2.9)	0.048 (1.9)	0.013 (0.5)	0.003 (0.1)	0.020 (0.8)	0.043 (1.7)	0.056 (2.2)	0.071 (2.8)	0.089 (3.5)	0.102 (4.0)	0.104 (4.1)
	0.119 (4.7)	0.104 (4.1)	0.074 (2.9)	0.046 (1.8)	0.018 (0.7)	0	0.025 (1.0)	0.048 (1.9)	0.056 (2.2)	0.071 (2.8)	0.089 (3.5)	0.097 (3.8)	0.106 (4.2)
Average	0.119 (4.7)	0.104 (4.1)	0.074 (2.9)	0.047 (1.85)	0.015 (0.6)	0.001 (0.05)	0.023 (0.9)	0.046 (1.8)	0.056 (2.2)	0.071 (2.8)	0.089 (3.5)	0.099 (3.9)	0.105 (4.15)

4. EFFECT OF CLAMPING ON THE EDGE OF THE GRID PLATE TEST MODEL

4.1. INTRODUCTION

Because the test model of the grid plate was clamped between two steel rings through eight preloaded bolts against the applied pressure loading, the boundary condition of the grid plate was not a simply supported case, and it was necessary to determine the effect of clamping in order to compare the results of testing with numerical and analytical methods. Table 3 shows that grid plate deflection is a function of bolt preload. The center deflection of the grid plate increased from 0.119 mm (4.7×10^{-3} in.) to 0.226 mm (8.9×10^{-3} in.) owing to the reduction of the bolt preload from 67.791 N·m (50 ft-lb) to 13.558 N·m (10 ft-lb). The test setup is shown in Fig. 16.

4.2. GRID PLATE AND SUPPORT RINGS

The free-body diagram of the grid plate and the support rings is shown in Fig. 17. In this figure, V and Q are the edge forces exerted at the corner edges of the support ring when the grid plate is subjected to a pressure loading. The rotation at the edge of the grid plate can be shown as

$$\theta = \frac{3(1 - \nu^*)pR^3}{2E^*H^3} - \frac{12(1 - \nu^*)R}{E^*H^3}(QH + tV) \quad . \tag{28}$$

4.3. SOLUTION OF SHORT CYLINDRICAL SHELL AND COMPATIBILITY

The lower support ring can be treated as a short cylinder[†] subjected to an edge force Q at the upper end and free at the lower end (Fig. 18).

[†]For a cylinder with $\ell < 3.1\sqrt{Rt}$.

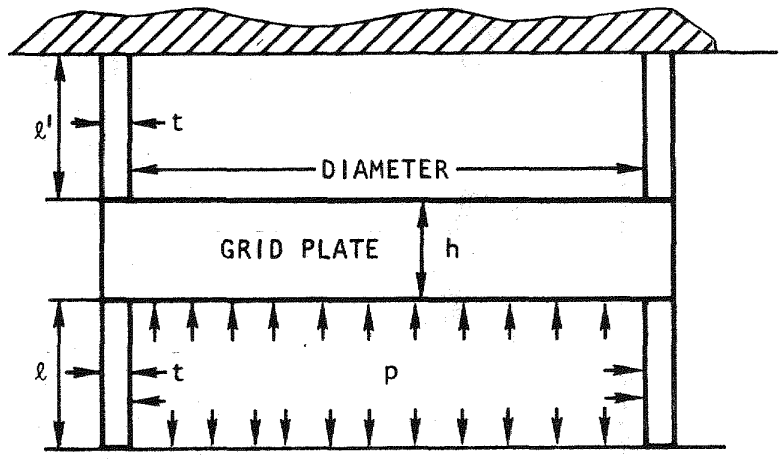

Fig. 16. Test setup

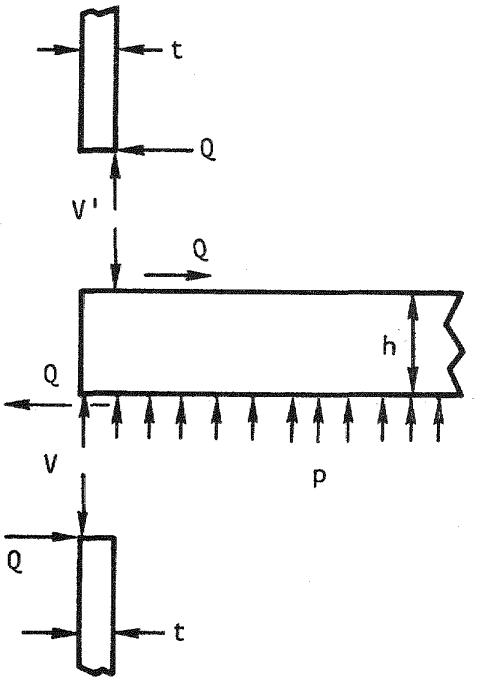

Fig. 17. Free-body diagram of the test grid plate and the support rings

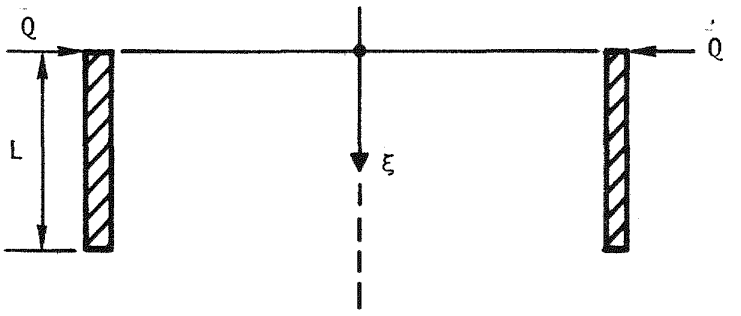

Fig. 18. Short cylinder subjected to an edge force

From Ref. 12, the exact formulas for a short cylindrical shell of uniform thickness subjected to an edge force is

$$u_r = - \frac{Q}{2Dk^3} \left[\frac{F_4}{F_1} F_7(\xi) - \frac{F_5}{F_1}(\xi) - \frac{F_6}{F_1} F_{16}(\xi) \right] \quad , \tag{29}$$

where

$$k = \frac{\sqrt[4]{3(1 - \nu^2)}}{\sqrt{Rt}} \quad ,$$

$$\xi = \frac{x}{\ell} \quad .$$

The factors F_i are defined as follows:

$$\left.\begin{aligned} F_1 &= \sinh^2 k\ell - \sin^2 k\ell \quad , \\ F_4 &= \sinh k\ell \cosh k\ell - \sin k\ell \cos k\ell \quad , \\ F_5 &= \sin^2 k\ell \quad , \\ F_6 &= \sinh^2 k\ell \quad , \\ F_7(\xi) &= \cosh k\ell\xi \cos k\ell\xi \quad , \\ F_{15}(\xi) &= \cosh k\ell\xi \sin k\ell\xi \quad , \\ F_{16}(\xi) &= \sinh k\ell\xi \cos k\ell\xi \quad . \end{aligned}\right\} \tag{30}$$

For the lower support cylinder, the radial deflection at the point of loading can be calculated:

$$\ell = 63.50 \text{ mm } (2.5 \text{ in.}) \quad ,$$

$$E = 206.8427 \times 10^3 \text{ MPa } (30 \times 10^6 \text{ psi}) \quad ,$$

$$D = \frac{Et^3}{12(1 - \nu^2)} = 0.1636 \times 10^5 \text{ N·m } (0.1448 \times 10^6 \text{ in.-lb}) \quad ,$$

$$F_1 = 7.0369 - 0.9828 = 6.0541 \quad ,$$

$$F_4 = (2.6527)(2.8349) - (0.9913)(-0.1313) = 7.6512 \quad ,$$

$$F_5 = 0.9828 \quad ,$$

$$F_6 = 7.0369 \quad ,$$

$$F_7(\xi)_{\xi=0} = 1 \quad ,$$

$$F_{15}(\xi)_{\xi=0} = 0 \quad ,$$

$$F_{16}(\xi)_{\xi=0} = 0 \quad ,$$

$$h = 91.44 \text{ mm } (3.6 \text{ in.}) \quad ,$$

$$R = 241.30 \text{ mm } (9.5 \text{ in.}) \quad ,$$

$$t = 9.525 \text{ mm } (0.375 \text{ in.}) \quad ,$$

$$\nu = 0.3 \quad .$$

Substituting these factors and parameters into Eq. 29 enables the expression for radial deflection to be reduced:

$$u_r = \frac{Q}{0.63160} \frac{7.6512}{6.0541} = \frac{2Q}{D}(1.6387 \times 10^{-5} \text{ m}^3) \simeq \frac{2Q}{D}(\text{in.}^3) \quad .(31)$$

When the test grid plate is deflected by the pressure loading, the support rings are also deformed. As shown in Fig. 19, the line a-b rotates as the grid plate and support rings deform. After the grid plate and support rings deform, the radial deflection of the ring can be written as

$$u_r = \overline{a\,a'} = \overline{b\,b'} = \overline{(bc)}\theta \quad .$$

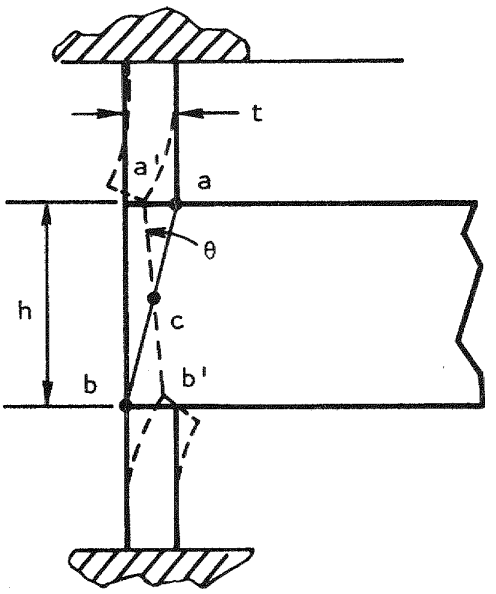

Fig. 19. Deformed grid plate model and support rings

Using Eqs. 28 through 30 and the relation of compatibility between the support ring and the grid plate enables the following relations to be derived: since

$$\theta = \frac{w}{\overline{bc}} \quad ,$$

$$bc = 1/2(h^2 + t^2)^{1/2} \quad ,$$

then

$$\frac{2}{\sqrt{h^2 + t^2}} \left(\frac{2Q}{D}\right) (1.6387 \times 10^{-5}\ m^3) = \frac{3(1 - \nu^*)pR^3}{2E^*h^3} - \frac{12(1 - \nu^*)R}{E^*h^3}(Qh + tV) \quad ,$$

or

$$Q\left[\frac{4(1.6387 \times 10^{-5}\ m^3)}{D\sqrt{h^2 + t^2}} + \frac{12(1 - \nu^*)Rh}{E^*h^3}\right] = \frac{3(1 - \nu^*)pR^3}{2E^*h^3} - \frac{12(1 - \nu^*)RtV}{E^*h^3} \quad , \qquad (32)$$

where $E^* = 1.379 \times 10^3$ MPa (0.2×10^6 psi) ,

$\nu^* = 0.76$,

$p = 413.68$ kPa (60 psi) .

The shear force V can be expressed in terms of the bolt preload $\bar{P}$ and the pressure load p on the grid plate model:

$$V = \frac{\bar{P} - \pi(R)^2 p}{2\pi(R)} \quad .$$

The eight bolts connecting the upper ring to the base plate were torqued to 67.791 N·m (50 ft-lb) each. Therefore, the total torque applied to the bolts is

$$T = 542.328 \text{ N·m } (4800 \text{ in.-lb}) \quad .$$

According to Stewart's estimate (Ref. 13), the preload P can be shown as

$$T = 0.2P \times (\text{diameter of the bolt in inches}) \quad ,$$

and the total preload of the bolts is

$$\bar{P} = \left(\frac{4{,}800 \times 2}{0.2}\right)(4.4482) = 2.135 \times 10^5 \text{ N } (48{,}000 \text{ lb}) \quad .$$

For a preload $\bar{P} = 2.135 \times 10^5$ N(48,000 lb) and a pressure load p = 413.68 kPa (60 psi), the shear force is

$$V = \frac{2.135 \times 10^5 \text{ N} - \pi(0.24448 \text{ m})^2(4.1369 \times 10^5 \text{ Pa})}{2\pi(0.24448 \text{ m})}$$

$$= 8.8422 \times 10^4 \text{ N/m } (504.903 \text{ lb/in.}) \quad .$$

Substituting the numerical values of all the constants plus the values of V and p into Eq. 32 yields

$$Q(4.3581 + 6.1065) \times 10^{-8} = (20.6399 - 5.6244) \times 10^{-4} \quad .$$

Therefore,

$$Q = \frac{15.0155}{10.4646} \times 10^4 = 1.4349 \times 10^4 \text{ N/m } (81.93 \text{ lb/in.}) \quad .$$

4.4. EFFECT OF CLAMPING ON CENTER DEFLECTION OF THE GRID PLATE

The terms w_1 and w_2 are defined as

w_1 = axial deflection at the center of the grid plate due to pressure loading p,

w_2 = reduction of axial deflection at the center of the grid plate due to clamping effect.

In mathematical form, w_1 and w_2 can be written as

$$w_1 = \frac{p}{64D} \frac{5 + \nu^*}{1 + \nu^*} R^4 \quad ,$$

$$w_2 = \frac{6(1 - \nu^*)R^2}{E^* h^3} (Qh + tV)$$

$$= \frac{R^2}{2D(1 + \nu^*)} \left[(1.4349 \times 10^4)(9.144 \times 10^{-2}) + (9.525 \times 10^{-3})(8.8422 \times 10^4) \right]$$

$$= \frac{R^2}{2D(1 + \nu^*)} (2154.29) \text{ m} \quad ,$$

$$\frac{w_2}{w_1} = \frac{(2154.29) \dfrac{R^2}{2D(1 + \nu^*)}}{\left(\dfrac{p}{64D}\right) \dfrac{(5 + \nu^*)}{(1 + \nu^*)} R^4}$$

$$= \frac{(2154.29)(32)}{p(5 + \nu^*)(R)^2} = \frac{(2154.29)(32)}{4.1369 \times 10^5 (5.76)(2.44475 \times 10^{-1})^2}$$

$$= 0.4834.$$

The clamping effect reduces the center deflection of the grid plate by 48.34%.

5. CONCLUSIONS

Using the analytical approach, the axial deflection at the center of the grid plate due to a 413.68-kPa (60-psi) uniform pressure loading is 0.2384 mm (9.387×10^{-3} in.); the finite-element model gives an axial deflection of 0.2337 mm (9.2×10^{-3} in.). These two results are considered to be in good agreement. However, the test measurement shows that the center deflection of the grid plate model is only 0.1194 mm (4.7×10^{-3} in.). As indicated in Section 4.4, the effect of clamping on the center deflection of the grid plate is approximately 48.34% of the total deflection; therefore, the center deflection of the grid plate should be 0.1194 mm (4.7×10^{-3} in.) + 0.2384 mm (9.387×10^{-3} in.) x 48.34% = 0.2346 mm (9.238×10^{-3} in.). Comparison of the adjusted testing result δ_{center} = 0.2346 mm (9.238×10^{-3} in.) with the analytical or finite-element result, indicates a less than 2% discrepancy among the three models.

For the case of a point 50.8 mm (2 in.) off the center under a pressure load of 413.68 kPa (60 psi), the axial deflections obtained by the analytical, testing, and finite-element methods are

Analytical

$$W_a = 0.2235 \text{ mm } (8.799 \times 10^{-3} \text{ in.}) \quad ,$$

Testing

$$W_t = 0.1067 \text{ mm } (4.2 \times 10^{-3} \text{ in.}) + 48.34\% \times 0.2235 \text{ mm } (8.799 \times 10^{-3} \text{ in.})$$

$$= 0.2147 \text{ mm } (8.453 \times 10^{-3} \text{ in.}) \quad ,$$

Finite-element

$$W_f = 0.2172 \text{ mm } (8.55 \times 10^{-3} \text{ in.}) \quad .$$

There is a 3.9% difference between the analytical and testing results and a 2.8% difference between the analytical and finite-element results.

For the case where r = 101.6 mm (4 in.) and p = 413.68 kPa (60 psi),

Analytical

$$W_a = 0.1812 \text{ mm } (7.134 \times 10^{-3} \text{ in.}) \quad ,$$

Testing

$$W_t = 0.0826 \text{ mm } (3.25 \times 10^{-3} \text{ in.}) + 48.34\%$$

$$\times 0.1812 \text{ mm } (7.134 \times 10^{-3} \text{ in.})$$

$$= 0.1702 \text{ mm } (6.699 \times 10^{-3} \text{ in.}) \quad ,$$

Finite-element

$$W_f = 0.1746 \text{ mm } (6.874 \times 10^{-3} \text{ in.}) \quad .$$

There is a 6.1% difference between the analytical and testing results and a 3.64% difference between the analytical and finite-element results.

For the case of r = 152.4 mm (6 in.)

Analytical

$$W_a = 0.1190 \text{ mm } (4.685 \times 10^{-3} \text{ in.}) \quad ,$$

Testing

$$W_t = 0.0546 \text{ mm } (2.15 \times 10^{-3} \text{ in.}) + 48.34\%$$

$$\times 0.1190 \text{ mm } (4.685 \times 10^{-3} \text{ in.})$$

$$= 0.1121 \text{ mm } (4.415 \times 10^{-3} \text{ in.}) \quad ,$$

Finite-element

$$W_f = 0.1135 \text{ mm } (4.467 \times 10^{-3} \text{ in.}) \quad .$$

There is a 5.76% difference between the analytical and testing results and a 4.75% difference between the analytical and finite-element results.

The three models are in good agreement, and the maximum discrepancy between them is about 6%. Because the clamping force induced by the preloaded bolts is not uniformly distributed along the edge of the grid plate, the testing results which are close to the results from the edge of the grid plate model are not accurate enough for comparative purposes. This is the reason that the comparisons were made only up to r = 152.4 mm (6 in.). The close agreement of the three models not only proves that the analytical derivation and finite-element model are correct, but also indicates that the equivalent Young's modulus E^* and equivalent Poisson's ratio ν^* obtained from Refs. 5 and 6 are accurate.

REFERENCES

1. Gardner, K. A., "Heat-Exchanger Tube-Sheet Design," J. Appl. Mech. 15, 377-385 (1948).
2. Gardner, K. A., "Heat-Exchanger Tube-Sheet Design - 2: Fixed Tube Sheets," J. Appl. Mech. 19, 159-166 (1952).
3. Gardner, K. A., "Heat-Exchanger Tube-Sheet Design - 3: U-Tube and Bayonet Tube Sheets," J. Appl. Mech. 27, 25-33 (1960).
4. Leknitskii, S. G., Theory of Elasticity of an Anisotropic Elastic Body, Holden-Day, San Francisco, 1963.
5. "ASME Boiler and Pressure Vessel Code," Section III, Article A-8000 (ASME 111/2).
6. Slot, T., "Stress Analysis of Thick Perforated Plates," Ph.D. Thesis, University of Technology Delft, The Netherlands, September 1972.
7. Love, A. E. H., A Treatise on the Mathematical Theory of Elasticity, 4th Ed., Dover, New York, 1974.
8. Timoshenko, S. P., and D. H. Young, Theory of Structure, 2nd ed., McGraw-Hill, New York, 1965.
9. Levesley, R. K., Matrix Method in Structural Analysis, Pergamon Press, New York, 1964.
10. Turner, M. J., et al., "Stiffness and Deflection Analysis of Complex Structures," J. Aeron. Sci. 23, 805-23 (1956).
11. Chang, K. H., A. S. Chuang, and C. E. Washington, "A Structural Analysis of the Gas-Cooled Fast Breeder Reactor Core Support," ERDA Report GA-A14098, General Atomic, June 1977.
12. Baker, E. H., L. Kovalevsky, and F. L. Rish, Structural Analysis of Shells, 1st ed., McGraw-Hill, New York, 1972.
13. ASME Handbook, McGraw-Hill, New York, 1953, pp. 171-177.